iScience

CellPress
OPEN ACCESS

Article

Clusterin is involved in mediating the metabolic function of adipose SIRT1

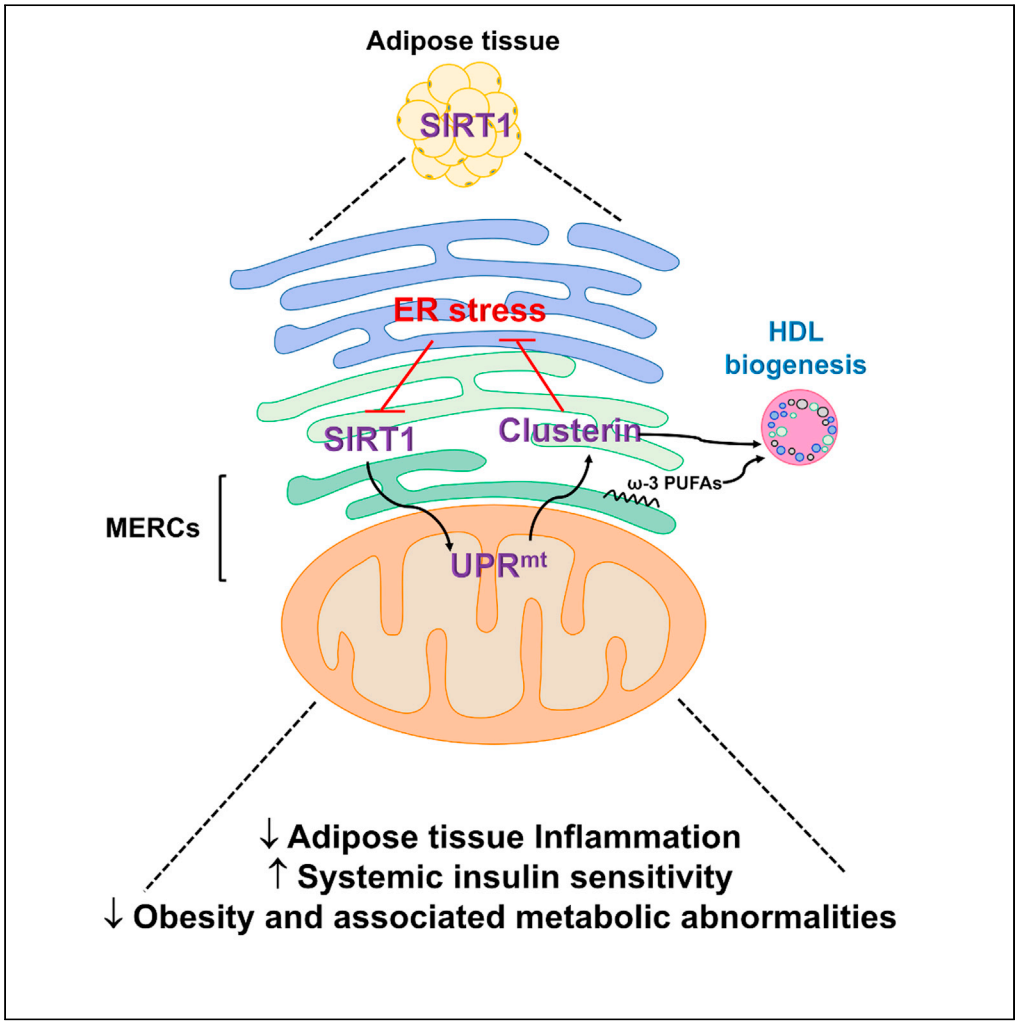

Pengcheng Zhang, Daniels Konja, Yiwei Zhang, ..., Ghader Bashiri, Alok Mitra, Yu Wang

yuwanghk@hku.hk

Highlights

Adipose SIRT1 triggers mitohormesis and UPR^{mt}, in turn upregulating clusterin

Adipose SIRT1 and clusterin regulate the protein and lipid compositions at MERCs

Adipose SIRT1 and clusterin reinforce UPR^{mt}-mediated anti-ER stress signaling

Adipose SIRT1 dysfunction causes obesity and associated metabolic abnormalities

Zhang et al., iScience *25*, 103709
January 21, 2022
https://doi.org/10.1016/j.isci.2021.103709

iScience

CellPress
OPEN ACCESS

Article

Clusterin is involved in mediating the metabolic function of adipose SIRT1

Pengcheng Zhang,[1,2] Daniels Konja,[1,2] Yiwei Zhang,[1,2] Aimin Xu,[1,2,3] In-Kyu Lee,[4,5] Jae-Han Jeon,[4,5] Ghader Bashiri,[6] Alok Mitra,[6] and Yu Wang[1,2,7,*]

SUMMARY

SIRT1 is a metabolic sensor regulating energy homeostasis. The present study revealed that mice with selective overexpression of human SIRT1 in adipose tissue (Adipo-SIRT1) were protected from high-fat diet (HFD)-induced metabolic abnormalities. Adipose SIRT1 was enriched at mitochondria-ER contacts (MERCs) to trigger mitohormesis and unfolded protein response (UPR^{mt}), in turn preventing ER stress. As a downstream target of UPR^{mt}, clusterin was significantly upregulated and acted together with SIRT1 to regulate the protein and lipid compositions at MERCs of adipose tissue. In mice lacking clusterin, HFD-induced metabolic abnormalities were significantly enhanced and could not be prevented by overexpression of SIRT1 in adipose tissue. Treatment with ER stress inhibitors restored adipose SIRT1-mediated beneficial effects on systemic energy metabolism. In summary, adipose SIRT1 facilitated the dynamic interactions and communications between mitochondria and ER, via MERCs, in turn triggering a mild mitochondrial stress to instigate the defense responses against dietary obesity-induced metabolic dysfunctions.

INTRODUCTION

In lower organisms, mild stresses of endoplasmic reticulum (ER) and mitochondria extend lifespan by initiating the unfolded protein responses (UPR^{ER} and UPR^{mt}, respectively) to restore the redox balance, cellular proteostasis, and metabolic homeostasis (Hetz et al., 2020; Labunskyy et al., 2014; Labbadia et al., 2017). ER stress and UPR^{ER} are triggered by increased demand for protein synthesis or accumulation of misfolded proteins (Hetz et al., 2020; Bhattarai et al., 2020). During UPR^{ER}, the sensor molecules anchored at the ER membrane, including inositol-requiring enzyme 1 (IRE1), activating transcription factor 6 (ATF6) and RNA-dependent protein kinase (PKR)-like ER kinase (PERK), are activated to transduce signals for the induction of various cellular responses in order to restore cellular and energetic homeostasis (Metcalf et al., 2020). However, prolonged ER stress increases the risk of metabolic diseases including obesity, insulin resistance, type 2 diabetes, and fatty liver injuries in mammals (Gregor et al., 2009; Bhattarai et al., 2020; Brown et al., 2020). In particular, adipose tissue dysfunction caused by ER stress and inflammation contributes to the pathophysiology of obesity-related metabolic disorders (Zatterale et al., 2019).

The function and stress signaling of mitochondria and ER are dynamically intertwined, especially in the context of metabolic regulation (Strzyz, 2019). Disturbed redox states in mitochondria lead to abnormal disulfide bond formation in ER and UPR^{ER} (Eisner et al., 2018; English et al., 2020). As powerhouse and building factory of the mammalian cells, mitochondria and ER are not only functionally but also structurally linked (Csordás et al., 2018; Zhang et al., 2021). The physical contacts between mitochondria and ER, referred to as MERCs, allow the exchange of different ions and metabolites, and play important roles in regulating calcium homeostasis, lipid metabolism, subcellular organelle structure, redox balance, and energy metabolism (Csordás et al., 2018). The formation, structure and function of MERCs are highly sensitive to nutritional status and hormonal stimulation (Cheng et al., 2020; Rieusset, 2018). Abnormalities in MERCs cause defects in insulin signaling and energy metabolism (Tubbs et al., 2018). Targeting mitochondria-ER communications via MERCs represents a promising therapeutic approach for various medical complications, including metabolic diseases.

SIRT1 (sirtuin 1) is a mammalian ortholog of the longevity regulator, yeast Sir2p, which catalyzes NAD^+-dependent deacetylation of various protein substrates (Pardo and Boriek, 2020). SIRT1 exerts potent

[1]The State Key Laboratory of Pharmaceutical Biotechnology, 21 Sassoon Road, Pokfulam, Hong Kong SAR, China

[2]Department of Pharmacology and Pharmacy, 21 Sassoon Road, Pokfulam, Hong Kong SAR, China

[3]Department of Medicine, The University of Hong Kong, Pokfulam, Hong Kong SAR, China

[4]Department of Internal Medicine, School of Medicine, Kyungpook National University Hospital, Daegu41944, South Korea

[5]Research Institute of Aging and Metabolism, Kyungpook National University, Daegu41404, South Korea

[6]School of Biological Sciences, University of Auckland, Auckland, New Zealand

[7]Lead contact

*Correspondence: yuwanghk@hku.hk

https://doi.org/10.1016/j.isci.2021.103709

anti-ageing activity in organ- and tissue-specific manners (Wang et al., 2012; Zu et al., 2010; Bai et al., 2012; Hui et al., 2017; Xu et al., 2015; Guo et al., 2019). As an energy and stress sensor, SIRT1 controls metabolic responses to nutrient availability. Treatment with SIRT1 activators improves insulin sensitivity, lowers plasma glucose, and increases mitochondrial capacity in diet-induced and genetically obese mice (Feige et al., 2008; Farghali et al., 2019; Strycharz et al., 2018). Previous studies suggest that overexpression of human SIRT1 selectively in adipose tissue improves energy homeostasis and impedes age-associated metabolic abnormalities (Xu et al., 2013, 2015). Loss-of-SIRT1 function selectively in the adipose tissue of mice promotes the development of metabolic aging and causes excessive lipid deposition in liver (Hui et al., 2017; Xu et al., 2015). The present study is aimed at investigating the mechanisms underlying adipose SIRT1-mediated protection against dietary obesity-induced metabolic abnormalities. The results demonstrated that SIRT1 was expressed and enriched at MERCs, in turn triggering mild mitochondrial stress but preventing dietary obesity-induced ER stress in adipose tissue. Clusterin, a chaperone that broadly protects against the pathogenic aggregation of proteins, played a critical role in SIRT1-mediated anti-ER stress signaling in adipose tissue and contributed to its beneficial effects on systemic energy homeostasis.

RESULTS

Adipo-SIRT1 are protected from dietary obesity-induced metabolic abnormalities

Compared to age-matched wild type (WT) littermates, mice with adipose tissue-specific overexpression of human SIRT1 (Adipo-SIRT1) exhibit enhanced insulin sensitivity and improved metabolic profiles (Xu et al., 2013, 2015). QPCR analyses revealed that the mRNA expression levels of *Clu* (clusterin) were significantly higher in epididymal adipose tissue of Adipo-SIRT1 than those of WT (Figure 1A). In liver, clusterin existed as ~70kDa precursor (pCLU), ~40kDa α (mCLUα) or ~30kDa β (mCLUβ) subunit of the mature protein. The expression levels of the precursor or mature forms of clusterin were not significantly different between liver samples of WT and Adipo-SIRT1 (Figure 1B). In adipose tissue, clusterin was expressed as ~75kDa pCLU, ~40kDa mCLUα or ~30kDa mCLUβ subunit of the mature protein (Figure 1B). Although the mRNA levels of *Clu* in adipose tissue were significantly lower, the protein expressions of this molecule were significantly higher than those of liver (Figures 1A and 1B). Moreover, the amount of the mature clusterin protein was significantly increased by overexpression of human SIRT1 in adipose tissue of Adipo-SIRT1 (Figure 1B).

Clusterin is a secreted glycoprotein eliciting cytoprotective roles in response to cellular stress (Garcia-Aranda et al., 2018; Park et al., 2014; Wilson and Zoubeidi, 2017). To investigate the role of clusterin in mediating the metabolic function of adipose SIRT1, $CKO^{Adipo-SIRT1}$ were generated by cross-breeding the clusterin knockout mice (CKO) with Adipo-SIRT1. Starting from the age of five weeks, WT, Adipo-SIRT1, CKO and $CKO^{Adipo-SIRT1}$ were fed with a high-fat diet (HFD) for 12 weeks. At the end of treatment, Adipo-SIRT1 exhibited significantly lower body weight (31.82 ± 1.91 vs 35.95 ± 1.12 g, $p<0.05$) and fat mass composition (17.82 ± 0.76% vs 22.35 ± 0.66%, $p<0.05$) than those of WT (Figure 1C). When compared to WT, the fasting levels of glucose (4.65 ± 0.13 vs 5.78 ± 0.18 mM, $p<0.05$), insulin (24.84 ± 3.62 vs 43.98 ± 10.98 μU/mL, $p<0.05$), triglyceride (0.56 ± 0.06 vs 0.82 ± 0.10 mM, $p<0.05$) and cholesterol (1.96 ± 0.62 vs 3.44 ± 0.29 mM, $p<0.05$) were all significantly lower in blood samples of Adipo-SIRT1 than those of WT (Figure 1D). By contrast, clusterin deficiency significantly increased the body weight (41.02 ± 0.80 and 39.35 ± 3.14 g, respectively), body fat mass composition (28.33 ± 1.79% and 26.08 ± 3.22%, respectively), circulating glucose (7.00 ± 0.48 and 6.92 ± 0.60 mM, respectively), insulin (109.88 ± 11.66 and 111.44 ± 8.29 μU/mL, respectively), triglyceride (1.14 ± 0.12 and 1.07 ± 0.11 mM, respectively) and cholesterol (4.23 ± 0.16 and 4.09 ± 0.26 mM, respectively) levels in CKO and $CKO^{Adipo-SIRT1}$(Figures 1C and 1D).

When compared to WT, the systemic insulin sensitivity and glucose tolerance were significantly enhanced in Adipo-SIRT1, as demonstrated by insulin (ITT) and intraperitoneal glucose (ipGTT) tolerance tests, respectively (Figures 1E and S1). Clusterin deficiency caused more severe insulin resistance and glucose intolerance in CKO, which were not prevented by overexpression of SIRT1 in adipose tissue of $CKO^{Adipo-SIRT1}$(Figures 1E and S1). Indirect calorimetry was performed to compare the oxygen consumption (VO_2), carbon dioxide production (VCO_2), respiratory exchange ratio (RER) and energy expenditure. When compared to WT, the VO_2 significantly increased during both dark (2751.33 ± 65.34 vs 3154.87 ± 127.55 mL/kg/h, $p<0.05$) and light (2501.98 ± 37.99 vs 2922.86 ± 142.66 mL/kg/h, $p<0.05$) cycles, whereas the VCO_2 were significantly increased during the dark cycles (2270.35 ± 72.71 vs 2585.01 ± 112.29 mL/kg/h, $p<0.05$) in Adipo-SIRT1 (Figure 1F). The RER of Adipo-SIRT1 during both dark (0.79 ± 0.01 vs 0.83 ± 0.01, $p<0.05$) and light (0.77 ± 0.01 vs 0.81 ± 0.01, $p<0.05$) cycles were significantly lower than those of WT (Figure 1G,*top*). The energy expenditure rates of Adipo-SIRT1 were significantly higher than those of WT during both dark (17.45 ± 0.42 vs 13.73 ± 0.68 kcal/kg/h, $p<0.05$) and

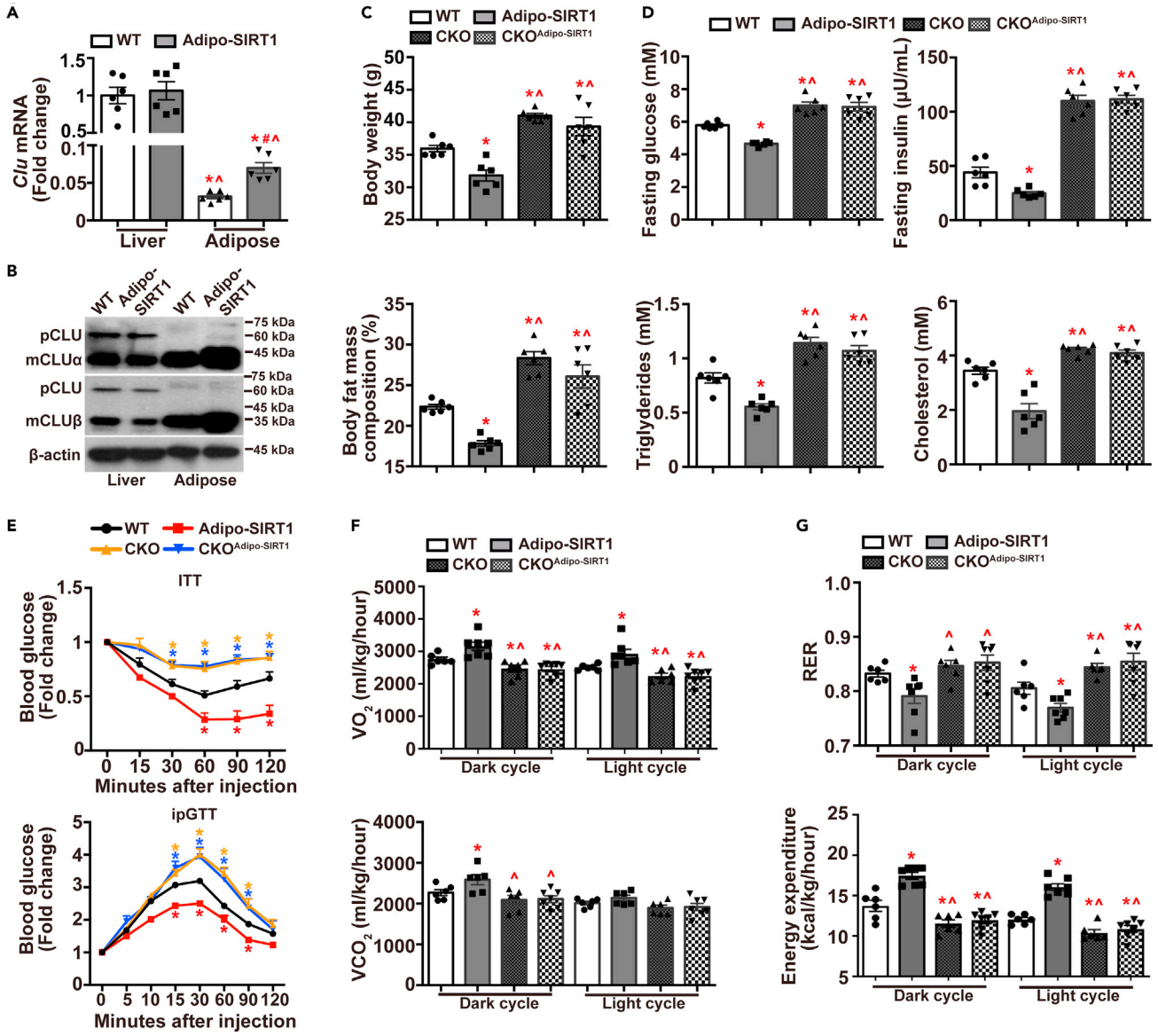

Figure 1. Overexpression of human SIRT1 increases clusterin expression selectively in adipose tissue and prevents the metabolic dysfunction induced by HFD

WT, Adipo-SIRT1, CKO and CKO$^{Adipo-SIRT1}$ were fed with HFD for 12 weeks. Various metabolic parameters were evaluated after starvation for 16 h. At the end of treatment, mice were sacrificed to collect serum and tissue samples for analyses.

(A) The mRNA expressions of *Clu* in liver and epididymal adipose tissues of WT and Adipo-SIRT1 were quantified by QPCR using 18S rRNA as an internal control. Results are presented as fold changes versus those in WT liver.

(B) Western blotting was performed to detect clusterin protein in liver and epididymal adipose tissues of WT and Adipo-SIRT1. Beta (β)-actin was detected as the loading control.

(C) Body weight (top) and fat mass composition (bottom) of WT, Adipo-SIRT1, CKO and CKO$^{Adipo-SIRT1}$ were measured for comparison.

(D) The circulating glucose, insulin, triglyceride and cholesterol levels in the four groups of mice were examined for comparison.

(E) Insulin (ITT) and intraperitoneal glucose tolerance (ipGTT) tests were performed in the four groups of mice for comparison.

(F) Indirect calorimetry was applied to obtain the average values of VO_2 and VCO_2 during the dark (19:00 pm - 7:00 am) and light (7:00 am−19:00 pm) cycles for comparison.

(G) RER and energy expenditure were calculated from the data of indirect calorimetry for comparison. Data are shown as means ± SEM. *, $p<0.05$ compared with WT liver or WT mice; #, $p<0.05$ compared with WT adipose tissue; ^, $p<0.05$ compared with Adipo-SIRT1 liver or Adipo-SIRT1 mice. (n = 6, One- or Two-way ANOVA)

light cycles (16.05 ± 0.40 vs 12.05 ± 0.24 kcal/kg/h, $p<0.05$) (Figure 1G,*bottom*). When compared to WT, the VO_2 of CKO and $CKO^{Adipo-SIRT1}$ significantly decreased during both dark (2466.54 ± 104.88 and 2455.88 ± 84.16 mL/kg/h, respectively) and light (2245.01 ± 80.78 and 2242.88 ± 92.12 mL/kg/h, respectively) cycles (Figure 1F). The RER of CKO (0.84 ± 0.01) and $CKO^{Adipo-SIRT1}$ (0.85 ± 0.02) during the light cycle were significantly higher than that of WT (Figure 1G,*top*). The energy expenditure rates of CKO and $CKO^{Adipo-SIRT1}$ during both dark (11.54 ± 0.46 and 11.99 ± 0.44 kcal/kg/h, respectively) and light (10.40 ± 0.40 and 10.92 ± 0.45 kcal/kg/h, respectively) cycles were significantly lower than those of WT (Figure 1G,*bottom*).

Overexpression of SIRT1 prevents HFD-induced ER stress in adipose tissue

When compared to WT, overexpression of SIRT1 significantly reduced the amounts of triglyceride and cholesterol in adipose tissue of Adipo-SIRT1 subjected to 12 weeks of HFD (Figure 2A). In adipose tissues of CKO and $CKO^{Adipo-SIRT1}$, the contents of triglyceride and cholesterol were significantly higher than those of WT and could not be reduced by overexpression of SIRT1 (Figure 2A). QPCR analyses revealed that the mRNA expression levels of *Ccl2* (monocyte chemoattractant protein-1), *Itgam* (integrin subunit alpha M), *Tgfb1* (transforming growth factor beta 1), and *Tnfα* (tumor necrosis factor alpha) were significantly decreased by overexpressing SIRT1 in adipose tissue of Adipo-SIRT1 (Figure 2B). Clusterin deficiency significantly increased the mRNA expression levels of *Ccl2*, *Itgam*, *Tgfb1*, and *Tnfα* in adipose tissues of CKO and $CKO^{Adipo-SIRT1}$(Figure 2B). Hematoxylin and eosin (H&E) staining revealed that overexpression of SIRT1 reduced the number of crown-like structures in adipose tissue of Adipo-SIRT1, whereas clusterin deficiency significantly increased those of CKO and $CKO^{Adipo-SIRT1}$(Figure 2C). The average size of adipocytes in adipose tissue of Adipo-SIRT1 (6424 ± 1352.5 μm2) was significantly smaller than that of WT (11,350 ± 2406.7 μm2). Clusterin deficiency significantly increased the average size of adipocytes in adipose tissues of CKO (28,545.3 ± 3760.8 μm2) and $CKO^{Adipo-SIRT1}$ (28011.8 ± 4869.1 μm2) (Figure 2C).

In adipose tissue of HFD-treated Adipo-SIRT1, the expression levels of genes involved in UPR^{ER}, including *Hspa5* [glucose-regulatory protein (GRP) 78], *Hsp90b1* (GRP94), *Ddit3* (C/EBP homologous protein), *Edem1* (ER degradation enhancing-mannosidase like protein 1), and *Dnajb9* (ER-localized DnaJ-domain containing protein 4) were significantly lower than those of the WT (Figure 2D). Without clusterin, HFD-induced UPR^{ER} were significantly enhanced in adipose tissues of CKO and $CKO^{Adipo-SIRT1}$(Figure 2D). When compared to those of WT, the total amount of PERK protein was significantly increased whereas the oligomerization capacity of this key ER stress sensor significantly decreased in adipose tissue of Adipo-SIRT1, accompanied by a significantly reduced phosphorylation of eukaryotic initiation factor 2α (eIF2α) (Figure 2E). In the absence of clusterin, both PERK oligomerization and eIF2α phosphorylation levels were significantly increased in adipose tissues of CKO and $CKO^{Adipo-SIRT1}$(Figure 2E). The total protein amount of IRE1 was significantly augmented in adipose tissue of Adipo-SIRT1. However, the levels of phosphorylated IRE1 were significantly inhibited by overexpression of SIRT1 in adipose tissue of Adipo-SIRT1 (Figure 2E).

Overexpression of SIRT1 attenuated, whereas clusterin deficiency promoted, the cleavage of activating transcription factor 6 (ATF6), another ER stress sensor (Bhattarai et al., 2020), in adipose tissue of Adipo-SIRT1 and CKO or $CKO^{Adipo-SIRT1}$, respectively (Figure 2F). When compared to WT, the protein amount of spliced X-box binding protein 1 (XBP1s), a product of IRE1 activation (Bhattarai et al., 2020), was significantly decreased in adipose tissue of Adipo-SIRT1 (Figure 2F). In adipose tissue of CKO and $CKO^{Adipo-SIRT1}$, the protein levels of XBP1s were significantly higher than that of WT (Figure 2F). In line with the QPCR results (Figure 2D), the protein expression of GRP78 was significantly downregulated in adipose tissue of Adipo-SIRT1 but upregulated in those of CKO and $CKO^{Adipo-SIRT1}$ (Figure 2F).

Overexpression of SIRT1 triggers mild mitochondrial stress in adipose tissue

QPCR analyses revealed that when compared to WT, the mRNA levels of genes involved in UPR associated with mitochondrial stress (UPR^{mt}), including *Hspe1* [heat shock protein (HSP) 10], *Hspd1* (HSP60), *Hspa9* (GRP75), *Lonp1* (LON peptidase 1), Nfe2 (nuclear factor erythroid 2–related factor 2), and *Hsf1* (heat shock transcription factor 1) were all significantly upregulated in adipose tissue of Adipo-SIRT1, irrespective of diet conditions (Figure 3A). Clusterin deficiency abolished SIRT1-induced UPR^{mt} in adipose tissue of $CKO^{Adipo-SIRT1}$ under HFD but not standard chow (STC) conditions (Figure 3A). Moreover, the expression levels of the UPR^{mt} genes were all significantly lower in mice without clusterin than WT under HFD (Figure 3A).

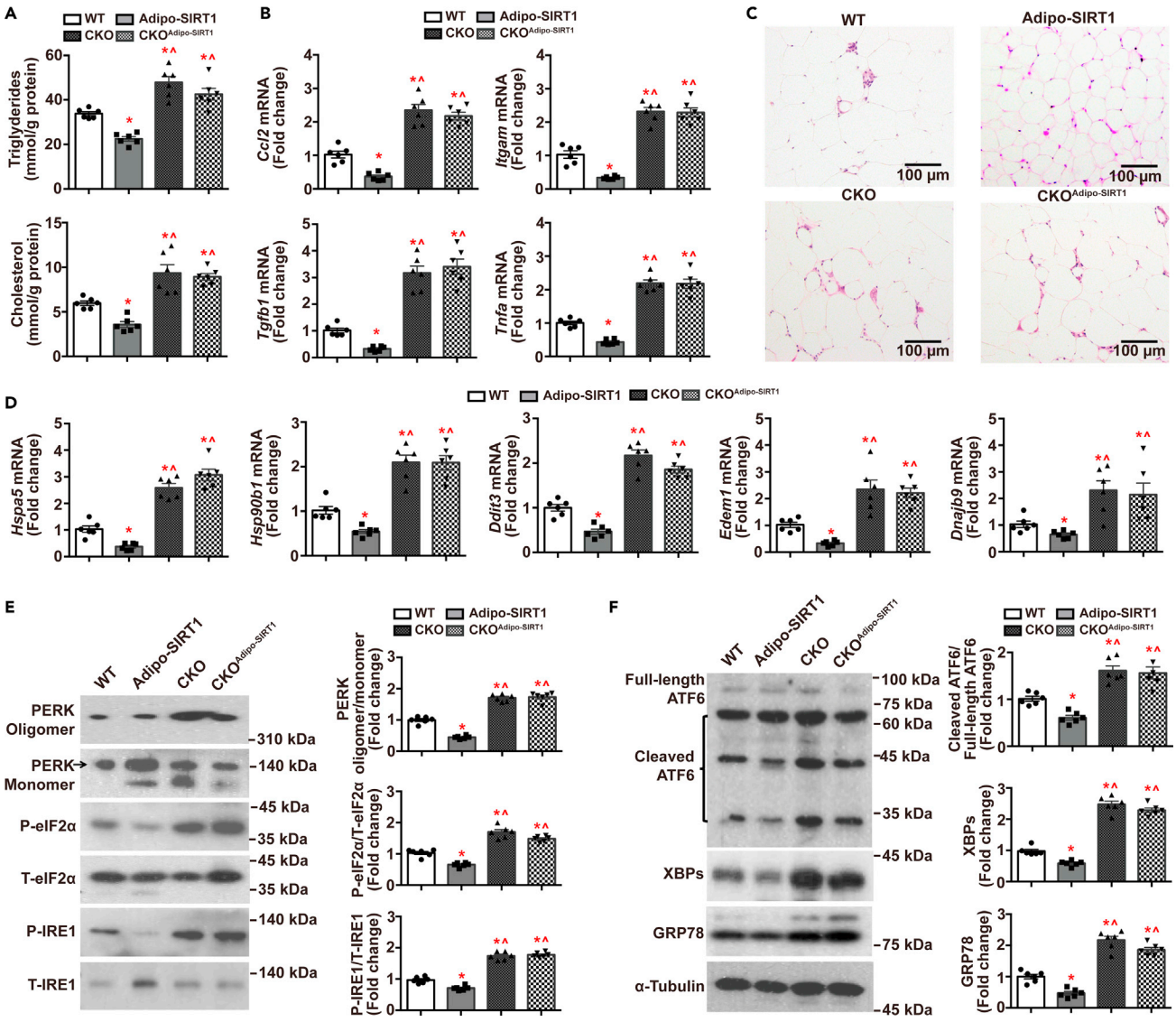

Figure 2. Overexpression of human SIRT1 prevents HFD-induced ER stress and inflammation in adipose tissue. WT, Adipo-SIRT1, CKO and CKO$^{Adipo-SIRT1}$ were fed with HFD for 12 weeks

At the end of treatment, after starvation for 16 h, mice were sacrificed and epididymal adipose tissues collected for the following examination.

(A) The contents of triglyceride and cholesterol were measured using commercial kits for comparison.

(B) QPCR was performed to evaluate the mRNA expression of genes involved in adipose tissue inflammation. The 18S rRNA was detected as an internal control for normalization. Results are presented as fold changes versus those of WT.

(C) H&E staining was applied on the tissue sections for histological analyses. Scale bar, 100 μm.

(D) QPCR was performed to evaluate the mRNA expression of genes involved in ER stress and UPR^{ER}. The 18S rRNA was detected as an internal control for normalization. Results are presented as fold changes versus those of WT.

(E) Western blotting was applied to analyze the ratios between oligomer and monomer of PERK, phosphorylated and total eIF2α, phosphorylated and total IRE1 for comparison.

(F) Western blotting was applied to analyze and compare the ratios between cleaved and full-length ATF6, as well as the expression levels of XBPs and GRP78 after normalization to α-tubulin. Data are shown as means ± SEM. *, $p<0.05$ compared with WT controls; ^, $p<0.05$ compared with those of Adipo-SIRT1. (n = 6, Two-way ANOVA)

In the presence of pyruvate and malate, the substrates of the electron transport chain (ETC) complex I, the mitochondria isolated from Adipo-SIRT1 produced significantly higher amounts of reactive oxygen species (ROS) than those of WT (Figure 3B,*left*). Overexpression of SIRT1 did not enhance the ROS production of mitochondria isolated from CKO$^{Adipo-SIRT1}$ under HFD condition (Figure 3B,*left*). Oxygen consumption

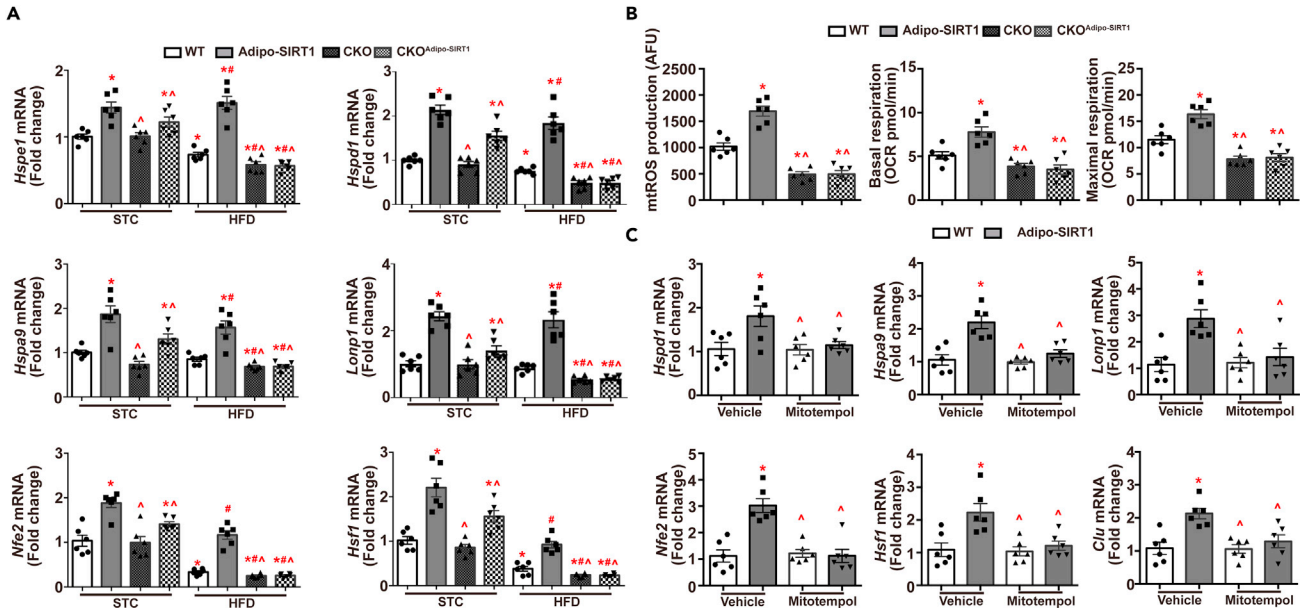

Figure 3. Overexpression of human SIRT1 selectively in adipose tissue induces mild mitochondrial stress and UPR^{mt}

WT, Adipo-SIRT1, CKO, and CKO$^{Adipo-SIRT1}$ were fed with either STC or HFD. At the age of 17 weeks, mice were sacrificed to collect the epididymal adipose tissues.

(A) QPCR was performed to analyze genes involved in mitochondrial stress and UPR^{mt}, including *Hspe1*, *Hspd1*, *Hspa9*, *Lonp1*, *Nfe2*, and *Hsf1*. The 18S rRNA was detected as an internal control for normalization. Results are presented as fold changes versus those of WT under STC.

(B) Mitochondria were isolated from adipose tissues of WT, Adipo-SIRT1, CKO and CKO$^{Adipo-SIRT1}$ under HFD. The mitochondrial ROS levels were measured as described in Methods (left). Oxygen consumption rate (OCR) was evaluated using a Seahorse Analyzer for calculating the basal (middle) and maximal (right) respirations for comparison.

(C) WT, Adipo-SIRT1, CTKO and CKO$^{Adipo-SIRT1}$ under HFD were subjected to a one-week treatment with vehicle or mitotempol (1 mg/kg/day, i.p.). Epididymal adipose tissues were collected for QPCR analyses of genes involved in mitochondrial stress and UPR^{mt}, including *Hspd1*, *Hspa9*, *Lonp1*, *Nfe2*, *Hsf1* and *Clu*. The 18S rRNA was detected as an internal control for normalization. Results are presented as fold changes versus those of WT treated with vehicle. Data are shown as means ± SEM. *, $p<0.05$ compared with WT STC (A), WT (B) or WT vehicle (C); #, $p<0.05$ compared with WT HFD; ^, $p<0.05$ compared with Adipo-SIRT1mice. (n = 6, Two-way ANOVA)

rate (OCR) of the isolated mitochondria was monitored using a Seahorse Analyzer. Overexpression of SIRT1 significantly enhanced both basal and maximal respiration in mitochondria isolated from adipose tissue of Adipo-SIRT1 (Figure 3B,*middle*and*right*). Without clusterin, overexpression of SIRT1 in adipose tissue did not increase the OCR in mitochondria isolated from adipose tissue of CKO$^{Adipo-SIRT1}$(Figure 3B, *middle* and *right*). When compared to WT, clusterin deficiency significantly reduced the ROS production and respiration in mitochondria isolated from adipose tissues of CKO and CKO$^{Adipo-SIRT1}$(Figure 3B).

Low levels of mitochondrial ROS production induce adaptive response, referred to as mitohormesis (Quirós et al., 2016; Anderson and Haynes, 2020; Melber and Haynes, 2018; Ristow and Schmeisser, 2011; Bárcena et al., 2018). To investigate whether mitohormesis was involved in the induction of UPR^{mt} by adipose SIRT1, mice under HFD were subjected to a one-week treatment with MitoTEMPOL, a mitochondria-targeted superoxide dismutase mimetic (Trnka et al., 2009). At the end of treatment, epididymal adipose tissues were collected for QPCR analyses. By selectively scavenging mitochondrial ROS, MitoTEMPOL abolished SIRT1-mediated UPR^{mt} and the upregulation of clusterin in adipose tissue of Adipo-SIRT1 (Figure 3C). The results suggested that SIRT1 induced mitohormesis, a mild mitochondrial stress signaling that upregulated the expression levels of clusterin.

SIRT1 and clusterin are expressed and enriched in MERCs of adipose tissue

Morphological analyses by transmission electron microscopy (TEM) revealed that in adipose tissues of Adipose-SIRT1, the ER tubular structures were widely distributed surrounding the mitochondria (Figure 4A, *left*). The average size of mitochondria in adipose tissue of Adipose-SIRT1 (61,685.11 ± 13,274.71 versus 173,663.61 ± 26,616.14 nm^2, $p<0.001$) was significantly smaller than that of WT (Figure 4A, *left*). Without clusterin, there were significantly less amounts of ER tubular structures and barely

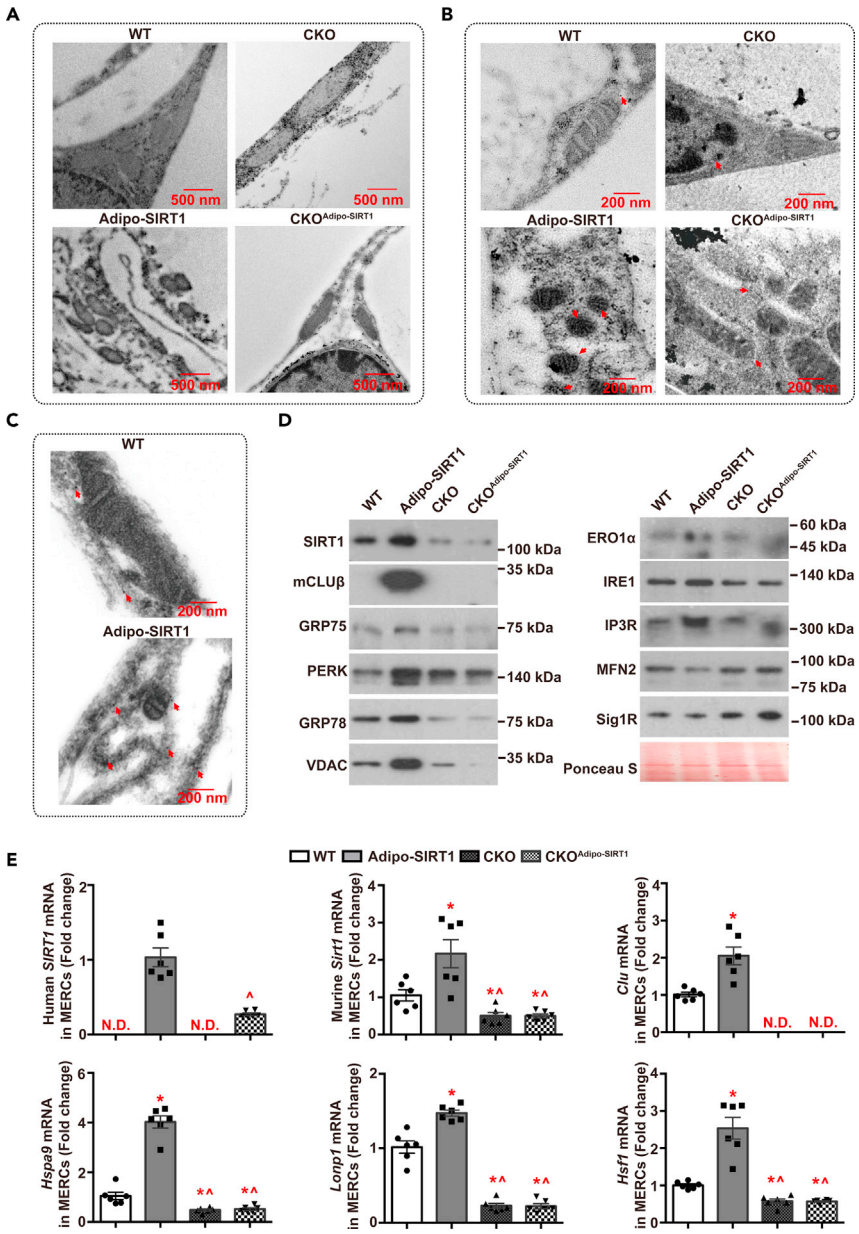

Figure 4. SIRT1 and clusterin are enriched in MERCs of adipose tissue

At the age of eight weeks, epididymal adipose tissues were collected from WT, Adipo-SIRT1, CKO and CKO$^{Adipo-SIRT1}$ under STC for the following analyses.

(A) TEM was applied to examine the ultrastructural features of mitochondria, ER and MERCs. Scale bar, 500 nm.

(B) Immuno-gold labeling was performed for TEM analyses of the subcellular localization of SIRT1 protein (red arrows). Scale bar, 200 nm.

(C) Immuno-gold labeling was performed for TEM analyses of the subcellular localization of clusterin protein (red arrows). Scale bar, 200 nm.

(D) MERCs were isolated from adipose tissue samples for Western blotting to analyze the amount of SIRT1, clusterin, GRP75, PERK, GRP78, VDAC, ERO1α, IRE1, IP3R, MFN2 and SigR1 proteins. Ponceau S staining was used for equal loading control.

(E) QPCR was performed for analyzing the mRNA transcript levels of *human SIRT1, murine Sirt1, Clu, Hspa9, Lonp1* and *Hsf1* in MERCs isolated from the four groups of mice. Data are shown as means ± SEM. *, $p<0.05$ compared with WT controls; ^, $p<0.05$ compared with Adipo-SIRT1. (n = 6, Two-way ANOVA)

any of those around the perimitochondrial region in adipose tissue of CKO and CKO$^{Adipo-SIRT1}$(Figure 4A, *right*). The localization of SIRT1 and clusterin protein was also examined by immunogold labeling. The results demonstrated that SIRT1 formed clusters on the ER membrane and/or at the interface between ER and mitochondria in adipose tissues of WT and Adipo-SIRT1 (Figure 4B). By contrast, there were significantly fewer amounts of electron-dense gold particles in the adipose tissue of CKO and CKO$^{Adipo-SIRT1}$(Figure 4B). The clusterin protein was abundantly localized on ER membranes, including those attached to mitochondria which were significantly increased in adipose tissues of Adipo-SIRT1 (Figure 4C).

The above data suggested that SIRT1 and clusterin were involved in the structural and functional regulation of ER and mitochondria. Next, MERCs were isolated from adipose tissue of WT, Adipo-SIRT1, CKO and CKO$^{Adipo-SIRT1}$ using a protocol described previously (Vance, 1990; Schreiner and Ankarcrona, 2017; Montesinos and Area-Gomez, 2020; Wieckowski et al., 2009). MERCs contained the resident proteins from both ER and mitochondria, but not those of cytosol (Figure S2). The yield of MERCs from the adipose tissue of Adipo-SIRT1 (71.76 $\pm$ 3.68 μg/g) was significantly higher whereas those of CKO and CKO$^{Adipo-SIRT1}$ (31.73 $\pm$ 2.61 and 29.37 $\pm$ 3.78 μg/g, respectively) were significantly lower than that of WT (42.00 $\pm$ 3.99 μg/g). Moreover, the MERCs of Adipo-SIRT1 contained more abundant proteins of SIRT1, clusterin, GRP75, PERK, GRP78, voltage-dependent anion channel (VDAC), endoplasmic reticulum oxidoreductase 1 alpha (ERO1α), IRE1 and inositol trisphosphate receptor (IP3R), but much less mitofusion 2 (MFN2) or sigma-1 receptor (Sig1R) than those of WT (Figure 4D). Without clusterin, overexpression of SIRT1 did not enhance the protein contents of GRP75, PERK, GRP78, VDAC, ERO1α, IRE1, and IP3R in MERCs of CKO$^{Adipo-SIRT1}$(Figure 4D). When compared to CKO, there were higher amounts of MFN2 and Sig1R in MERCs isolated from the adipose tissue of CKO$^{Adipo-SIRT1}$(Figure 4D).

Interestingly, the mRNA transcripts of human *SIRT1* and murine *Sirt1* as well as genes involved in UPR^{mt} were detected at MERCs (Figure 4E). The mRNA levels of human *SIRT1* were significantly lower at MERCs of CKO$^{Adipo-SIRT1}$ than that of Adipo-SIRT1 (Figure 4E). The endogenous murine *Sirt1* mRNA transcript was significantly increased at MERCs isolated from adipose tissue of Adipo-SIRT1, but decreased in those of CKO and CKO$^{Adipo-SIRT1}$(Figure 4E). When compared to WT, the mRNA levels of *Clu*, *Hspa9, Lonp1* and *Hsf1* were significantly augmented at MERCs isolated from the adipose tissue of Adipo-SIRT1, whereas clusterin deficiency significantly reduced the amount of mRNA transcripts involved in UPR^{mt} at MERCs isolated from the adipose tissue of CKO and CKO$^{Adipo-SIRT1}$(Figure 4E).

Overexpression of SIRT1 increased omega-3 polyunsaturated fatty acids (ω-3 PUFAs) in MERCs of adipose tissue

Gas chromatography-mass spectrometry (GC-MS) was applied to analyze the lipid composition of MERCs isolated from epididymal adipose tissues of WT, Adipo-SIRT1, CKO and CKO$^{Adipose-SIRT1}$. The results revealed that the contents of ω-3 PUFAs, including eicosapentaenoic acid (EPA; C20:5 n-3), docosapentaenoic acid (DPA; C22:5 n-3) and docosahexaenoic acid (DHA; C22:6 n-3), were all significantly higher in MERCs of Adipo-SIRT1 but significantly lower in those of CKO and CKO$^{Adipo-SIRT1}$ than WT (Figure 5A). On the other hand, the cholesterol content was significantly decreased in MERCs of Adipo-SIRT1 but augmented in those of CKO and CKO$^{Adipo-SIRT1}$, when compared to WT (Figure 5A). Further analyses revealed that the percentage contents of ω-3 PUFAs were more than two-folds higher in the phospholipid but not in the neutral lipid fractions extracted from MERCs of Adipo-SIRT1 than those of WT (Figure 5B). In samples from CKO and CKO$^{Adipo-SIRT1}$, the percentage contents of ω-3 PUFAs were significantly reduced mainly in phospholipid, but not neutral lipid fractions (Figure 5B).

Compared with WT, the amount of conjugated, but not free ω-3 PUFAs, was significantly increased in the adipose tissue of Adipo-SIRT1 (Table S1). The ratios between conjugated and free ω-3 PUFAs were 14.63 $\pm$ 4.22, 8.08 $\pm$ 0.86 and 3.46 $\pm$ 0.69 for EPA, DPA, and DHA, respectively, in adipose tissue of Adipo-SIRT1, which were significantly higher than those of WT (8.09 $\pm$ 1.06, 6.24 $\pm$ 0.79 and 2.23 $\pm$ 0.35, respectively). The amounts of both conjugated and free ω-3 PUFAs were significantly increased in liver of Adipo-SIRT1 (Table S2). When compared to WT, the conjugated ω-3 PUFAs were significantly decreased in liver and epididymal adipose tissues of both CKO and CKO$^{Adipo-SIRT1}$(Tables S1 and S2). The amounts of free ω-3 PUFAs in adipose tissues of CKO and CKO$^{Adipo-SIRT1}$ were significantly higher than those of WT (Table S1). In adipose tissues of CKO and CKO$^{Adipo-SIRT1}$, the ratios between conjugated and free ω-3 PUFAs for EPA (4.26 $\pm$ 0.67 and 2.99 $\pm$ 0.75, respectively), DPA (2.61 $\pm$ 0.50 and

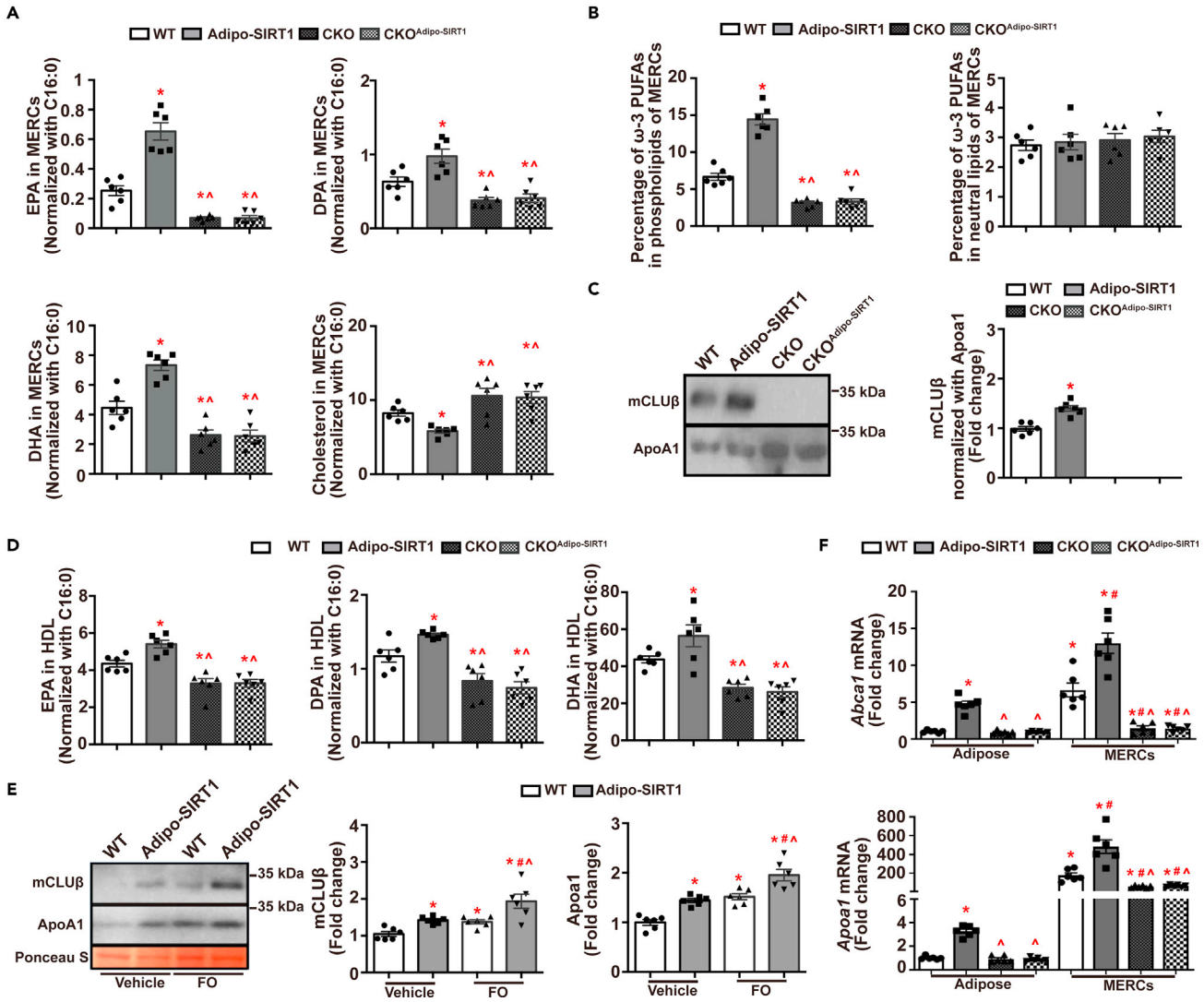

Figure 5. Increased contents of ω3-PUFAs in MERCs of adipose tissue and HDL particle of Adipo-SIRT1

WT, Adipo-SIRT1, CKO, and CKO$^{Adipo-SIRT1}$ were fed with HFD for 12 weeks. At the end of treatment, after starvation for 16 h, serum, epididymal adipose tissue and liver were collected for the following analyses.

(A) MERCs were isolated from epididymal adipose tissue. GC-MS was applied to measure the contents of EPA, DPA, DHA and cholesterol as described in the Methods for comparison.

(B) Phospholipids and neutral lipids were fractionated from MERCs. GC-MS was applied to measure the percentage of ω-3 PUFAs for comparison.

(C) HDL particles were isolated from serum samples of WT and Adipo-SIRT1. Western blotting was performed to examine the protein contents of clusterin and ApoA1, the ratios of which were calculated for comparison.

(D) GC-MS was applied to compare the amount of EPA, DPA and DHA in the isolated HDL particles.

(E) Explant cultures of epididymal adipose tissue were prepared from WT and Adipo-SIRT1. After 20 min treatment with vehicle or fish oil [FO; 0.6% (v/v)], the conditioned media were collected for Western blotting to examine the protein amount of clusterin and ApoA1. Ponceau S staining was used for total protein normalization.

(F) QPCR was performed for measuring the mRNA expression of genes involved in the biogenesis of HDL, including *Abca1* and *Apoa1*, in epididymal adipose tissue and MERCs. The 18S rRNA was detected as an internal control for normalization. Results are presented as fold changes versus those in adipose tissue of WT. Data are shown as means ± SEM. *, $p<0.05$ compared with corresponding WT controls; #, $p<0.05$ compared with WT FO (E) or WT MERCs (F); ^, $p<0.05$ compared with Adipo-SIRT1. (n = 6, Two-way ANOVA)

1.90 ± 0.16, respectively) and DHA (0.98 ± 0.13 and 0.89 ± 0.11, respectively) were significantly lower than those of WT. The ratios between conjugated and free ω-3 PUFAs in livers of all mice groups were not significantly different.

In human blood circulation, over 20% of clusterin is packaged within the high-density lipoprotein (HDL) particles. Low clusterin levels in HDL are associated with insulin resistance, obesity and dyslipoproteinemia (Hoofnagle et al., 2010; Rull et al., 2015). In HDL particles isolated from Adipo-SIRT1, there were significantly increased amounts of clusterin protein (Figure 5C). Moreover, the contents of ω-3 PUFAs, including EPA, DPA, and DHA, were all significantly higher in HDL particles isolated from Adipo-SIRT1 (Figure 5D). In the absence of clusterin, the ω-3 PUFAs were significantly decreased in HDL particles isolated from CKO and CKO$^{Adipo-SIRT}$(Figure 5D). Under both basal and fish oil-stimulated conditions, the protein amounts of secreted clusterin and apolipoprotein A1 (ApoA1), were significantly higher in the conditional media collected from the adipose explant culture of Adipo-SIRT1 than those of WT (Figure 5E). QPCR analyses revealed that the mRNA levels of *Abca1* (ATP binding cassette subfamily A member 1, a transporter responsible for cholesterol efflux) and *Apoa1* (ApoA1, a major protein component of HDL particle) were significantly higher in adipose tissue and MERCs of Adipo-SIRT1 than those of WT (Figure 5F). Clusterin deficiency significantly reduced the amount of *Abca1* and *Apoa1* transcripts in MERCs but not adipose tissues of CKO and CKO$^{Adipo-SIRT1}$, when compared to WT (Figure 5F).

SIRT1 expression is downregulated by hyper-activated ER-stress signaling in adipose tissue

QPCR analyses revealed that the mRNA transcript of the transgenic human *SIRT1* was present in adipose tissue, but not liver, of Adipo-SIRT1 and CKO$^{Adipo-SIRT1}$(Figure 6A). The expression levels of human *SIRT1* were significantly lower in adipose tissue of CKO$^{Adipo-SIRT1}$ than that of Adipo-SIRT1 (Figure 6A). The endogenous murine *Sirt1* expression was significantly increased by overexpressing human SIRT1 in the adipose tissue of Adipo-SIRT1 and CKO$^{Adipo-SIRT1}$(Figure 6B). When compared with those under STC (Figures 6A and 6B), the expression levels of human *SIRT1* and murine *Sirt1* were decreased by ~40-50% in adipose tissues of mice treated with HFD (Figures 6C and 6D). Clusterin deficiency further decreased the expression levels of human *SIRT1* and murine *Sirt1* by ~45-80% in mice treated with HFD (Figures 6C and 6D). Both HFD and clusterin deficiency did not significantly alter the mRNA expression levels of murine *Sirt1* in the liver, which was much lower (~60%) than those in adipose tissue of WT (Figure 6D). Consistently, when compared to WT, the protein expression levels of SIRT1 were significantly increased in adipose tissue of Adipo-SIRT1 under both STC and HFD conditions (Figure 6E). Under STC, the protein expression levels of SIRT1 in adipose tissue of CKO$^{Adipo-SIRT1}$ were significantly higher than those of CKO (Figure 6E). However, under HFD, the protein expression levels of SIRT1 in adipose tissues of CKO and CKO$^{Adipo-SIRT1}$ were significantly lower than all other groups of samples (Figure 6E).

The above data suggested that the significantly reduced expression of SIRT1 might be caused by the hyper-activated ER stress in adipose tissues of CKO and CKO$^{Adipo-SIRT1}$. Since ω-3 PUFAs are well-known ER stress inhibitors (Lepretti et al., 2018; Okada et al., 2018), WT, Adipo-SIRT1, CKO or CKO$^{Adipo-SIRT1}$ were given a single dose (by oral gavage) of 0.2 mL fish oil containing ~18% EPA and ~12% DHA. Before and at three, six, or nine hours after fish oil oral gavage, epididymal adipose tissue and liver were collected for GC-MS analyses. The results demonstrated that the levels of ω-3 PUFAs were significantly augmented in adipose tissue of Adipo-SIRT1, but not those of CKO or CKO$^{Adipo-SIRT1}$, when compared to WT (Figure 7A, *top*). Compared to adipose tissue, treatment with fish oil did not significantly change the content of ω-3 PUFAs in liver samples of all four groups of mice (Figure 7A, *bottom*). The MERCs were also collected for GC-MS and Western blotting analyses. The amounts of EPA, DPA, and DHA were also significantly augmented in MERCs of WT and Adipo-SIRT1, with the latter exhibiting much higher levels (Figure 7B). The protein levels of SIRT1, NDUFS2, PERK, IRE1, and VDAC were progressively increasing in MERCs of both WT and Adipo-SIRT1 at three and six hours after the bolus treatment with fish oil (Figure 7C). By contrast, the protein contents of GRP78 and clusterin were slightly decreased in MERCs of WT and Adipo-SIRT1 at six hours after the bolus treatment with fish oil (Figure 6C). There were barely any changes for both the ω-3 PUFAs levels and protein contents in MERCs of CKO and CKO$^{Adipo-SIRT1}$(Figures 7B and S3). Treatment with fish oil stimulated the mRNA expressions of human *SIRT1*, murine *Sirt1*, *Clu*, and other UPR^{mt} genes in adipose tissue of Adipo-SIRT1 but not those of CKO$^{Adipo-SIRT1}$(Figure 7D).

Inhibition of ER stress restores metabolic functions mediated by adipose SIRT1

To further investigate the effects of ER stress signaling on SIRT1 expression in adipose tissue, CKO and CKO$^{Adipo-SIRT1}$ under HFD were subjected to a one week treatment with vehicle, tauroursodeoxycholic acid (TUDCA; 100 mg/kg/day, i.p.) or IRE1 inhibitor mixture [4μ8c (10 mg/kg/day, i.p.), MKC8866 (20 mg/kg/day, i.p.), STF083010 (30 mg/kg/day, i.p.) and KIRA6 (5 mg/kg/day, i.p.)]. At the end of treatment, the epididymal adipose tissues were collected to measure the mRNA expression levels of human

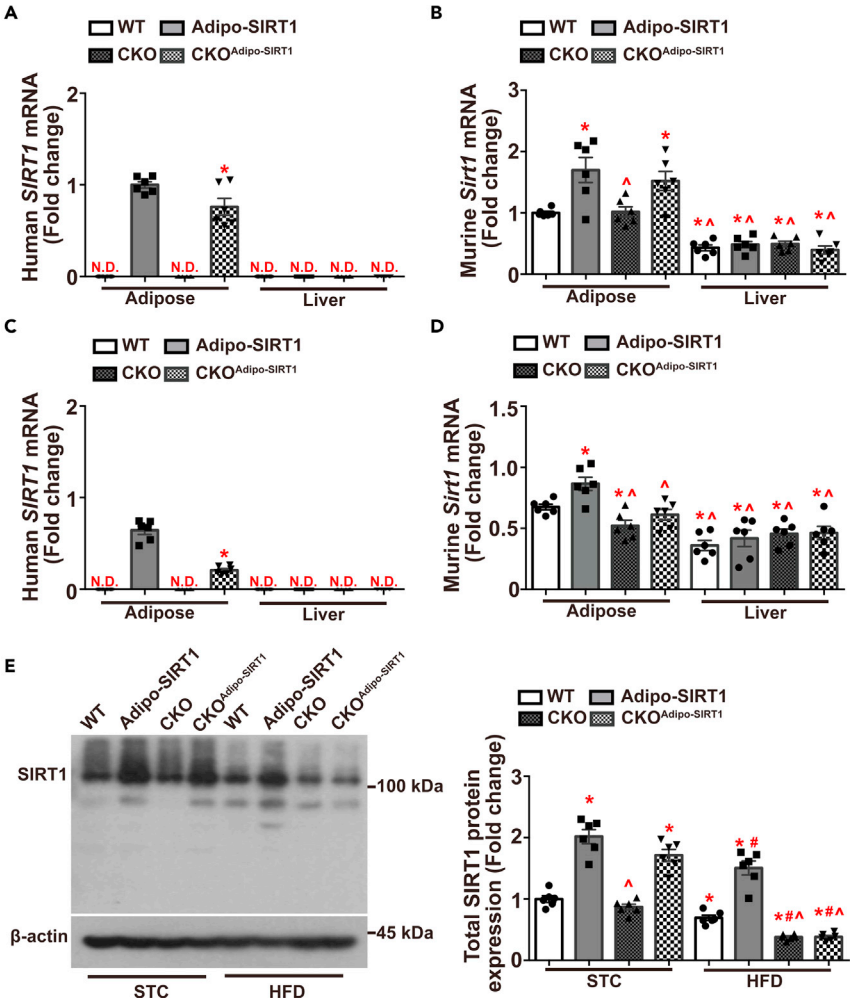

Figure 6. The expression levels of adipose SIRT1 are downregulated by HFD and clusterin deficiency

Epididymal adipose and liver tissues were collected from 17 weeks old WT, Adipo-SIRT1, CKO and CKO$^{Adipo-SIRT1}$ under STC or HFD for analysis.

(A) QPCR was performed to measure the mRNA expression levels of human SIRT1 under STC. The 18S rRNA was detected as an internal control for normalization. The results are presented as fold changes versus the expression level in adipose tissue of Adipo-SIRT1 under STC.

(B) QPCR was performed to measure the mRNA expression levels of murine *Sirt1* under STC. The 18S rRNA was detected as an internal control for normalization. The results are presented as fold changes versus the expression level in adipose tissue of WT under STC.

(C) QPCR was performed to measure the mRNA expression levels of human *SIRT1* under HFD. The 18S rRNA was detected as an internal control for normalization. The results are presented as fold changes versus the expression level in adipose tissue of Adipo-SIRT1 under STC.

(D) QPCR was performed to measure the mRNA expression levels of murine *Sirt1* under HFD. The 18S rRNA was detected as an internal control for normalization. The results are presented as fold changes versus the expression level in adipose tissue of WT under STC.

(E) Western blotting was performed to quantify the total protein amount of SIRT1 in epididymal adipose tissues. Data are shown as means ± SEM. *, $p<0.05$ compared with adipose tissue of Adipo-SIRT1 (A and C) or WT (B and D), or WT STC (E); #, $p<0.05$ compared with WT HFD; ^, $p<0.05$ compared with corresponding Adipo-SIRT1. (n = 6, One- or Two-way ANOVA)

SIRT1 and murine *Sirt1*. The results demonstrated that administration of TUDCA significantly increased the mRNA levels of both human *SIRT1* and murine *Sirt1* in adipose tissues of these animals (Figure S4). Treatment with the IRE1 inhibitors also significantly increased the mRNA expression of murine *Sirt1* and human *SIRT1*, but to a less extent than TUDCA (Figure S4).

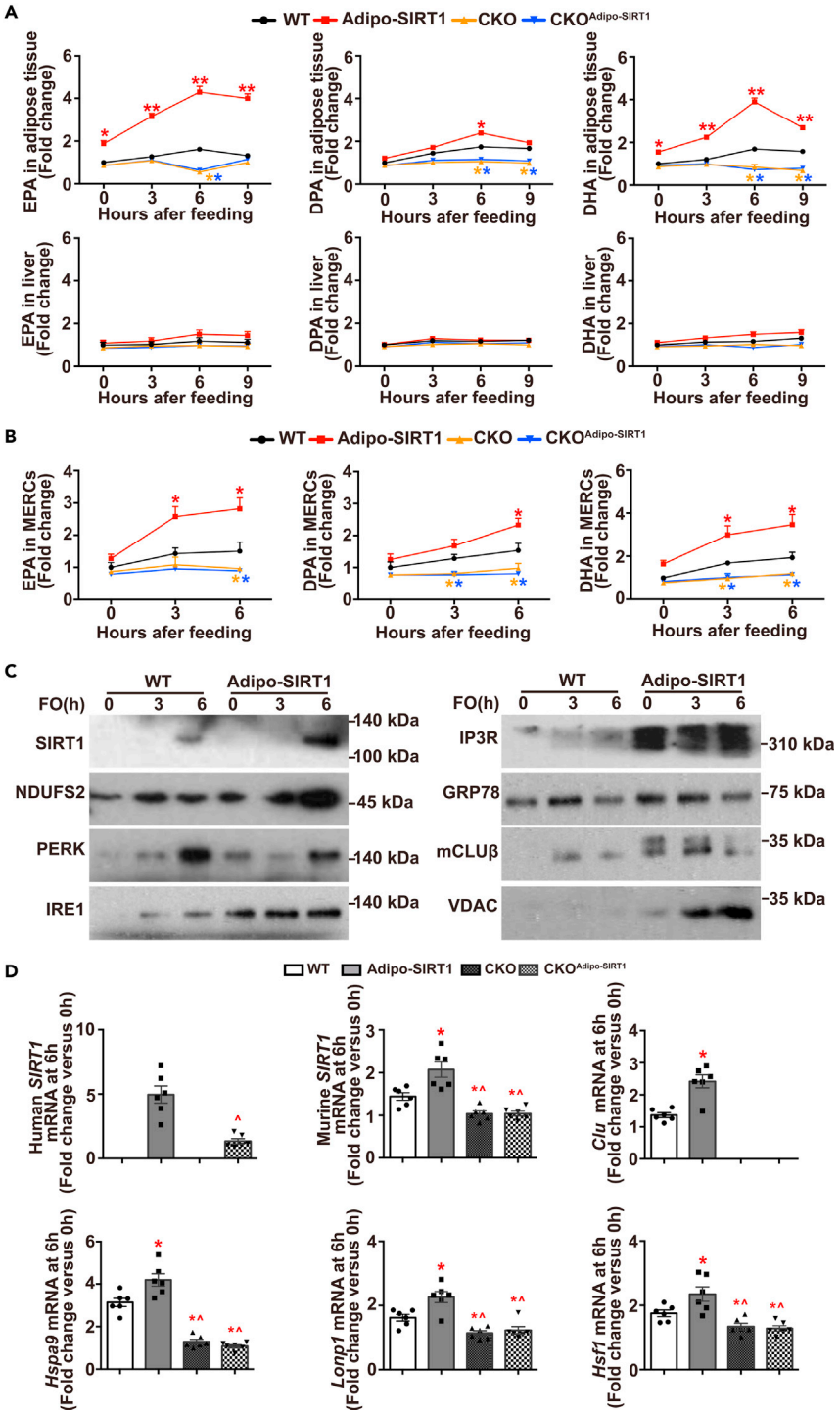

Figure 7. Overexpression of SIRT1 facilitates the incorporation of ω3-PUFAs in MERCs of adipose tissue

WT, Adipo-SIRT1, CKO and CKO$^{Adipo-SIRT1}$ under STC were treated with one dose of fish oil by oral gavage. Epididymal adipose tissue and liver were collected before (time zero) or three, six, and nine hours after oral gavage for analyses.

(A) GC-MS was applied to measure the total amount of EPA, DPA and DHA in adipose tissue (top) or liver (bottom) samples. Results were presented as fold changes versus those of WT at time zero.

(B) GC-MS was applied to measure the amount of EPA, DPA and DHA in MERCs isolated from the adipose tissue samples. All values were normalized to those of the C19:0 internal control for comparison.

Figure 7. *Continued*

(C) Western blotting was performed for analyzing the protein contents of SIRT1, NDUFS2, PERK, IRE1, IP3R, GRP78, clusterin and VDAC in MERCs isolated from adipose tissues of WT and Adipo-SIRT1.

(D) QPCR was performed to measure the mRNA levels of human *SIRT1*, murine *Sirt1*, *Clu*, *Hspa9*, *Lonp1* and *Hsf1* in adipose tissue samples collected before or at nine hours after oral gavage. The 18S rRNA was detected as an internal control for normalization. Results are presented as fold changes versus samples collected at time zero. Data are shown as means ± SEM. *, $p<0.05$, compared with corresponding WT controls; ^, $p<0.05$ compared with Adipo-SIRT1 (n = 6, One- or Two-way ANOVA)

Next, TUDCA was used for long-term treatment in CKO and $CKO^{Adipo-SIRT1}$ mice under HFD, starting from the age of 11 weeks. After six weeks of daily intraperitoneal injections, TUDCA significantly reduced the body fat mass composition and improved glucose as well as insulin tolerance in CKO and $CKO^{Adipo-SIRT1}$(Figure 8A and B). The mRNA expression levels of genes involved in ER stress, including *Hspa5*, *Ddit3*, *Xbps*, and *Hsp90b1*, were all significantly decreased by TUDCA treatment in adipose tissues of CKO and $CKO^{Adipo-SIRT1}$(Figure 8C), which showed significantly reduced number of crown-like structures (Figure 8D). The effects of TUDCA treatment in $CKO^{Adipo-SIRT1}$ were more significant than those of CKO (Figures 8A–8D), which were in line with the higher expression of SIRT1 in adipose tissue of the former group (Figure 6).

After 12 weeks of HFD, the amount of lipids accumulated in the liver of Adipo-SIRT1 was significantly lower than that of WT, as demonstrated by H&E and Oil Red O staining (Figure S5,*top*), as well as the biochemical measurement of triglyceride and cholesterol levels (Figure 8E, *left*). The mRNA expression levels of *Pparα* (peroxisome proliferator-activated receptor alpha) and *Fgf21* (fibroblast growth factor 21) were significantly increased in the liver of Adipo-SIRT1 (Figure 8E, *right*). Clusterin deficiency caused severe steatohepatitis (Figure S5, *middle*), and significantly increased hepatic contents of triglyceride and cholesterol (Figure 8E, *left*), but prevented adipose SIRT1-mediated upregulation of *Pparα* and *Fgf21* in the liver of $CKO^{Adipo-SIRT1}$(Figure 8E, *right*). Compared to WT, the circulating levels of liver injury markers, including alanine transaminase (ALT) and aspartate aminotransferase (AST), were significantly augmented in CKO and $CKO^{Adipo-SIRT1}$(Figure 8F, *left*). The mRNA expression levels of fibrosis-associated genes, including *Col1a1* (collagen type I alpha 1 chain) and *Tgfb1* (transforming growth factor 1), were both significantly increased in livers of CKO and $CKO^{Adipo-SIRT1}$(Figure 8F,*right*).

TUDCA treatment significantly attenuated HFD-induced steatohepatitis (Figure S5,*bottom*), reduced hepatic contents of triglyceride and cholesterol (Figure 8E, *left*), and restored adipose SIRT1-mediated upregulation of *Pparα* and *Fgf21* in liver of $CKO^{Adipo-SIRT1}$(Figure 8E,*right*). The circulating levels of ALT and AST as well as the hepatic expressions of *Col1a1* and *Tgfb1* were all significantly reduced by TUDCA treatment (Figure 8F). Compared to CKO, TUDCA treatment not only restored but also significantly enhanced adipose SIRT1-mediated hepatoprotective functions in $CKO^{Adipo-SIRT1}$, which showed similar levels of lipid contents in liver, circulating ALT and AST, hepatic expression of *Pparα*, *Fgf21*, *Col1a1* and *Tgfb1* as those of Adipo-SIRT1 (Figures 8E and 8F).

DISCUSSION

Adipose tissue dysfunction represents a major risk factor contributing to the development of obesity and associated metabolic abnormalities, including insulin resistance and type 2 diabetes (Zatterale et al., 2019). The present study demonstrated that overexpression of human SIRT1 in adipose tissue prevented dietary obesity-induced obesity, insulin resistance, hyperglycemia, dyslipidemia, and metabolic dysfunction-associated fatty liver disease (MAFLD). In adipose tissue, SIRT1 triggered a mild mitochondrial stress under both STC and HFD conditions, but inhibited dietary obesity-induced ER stress and inflammation. In the absence of clusterin, however, overexpression of adipose SIRT1 failed to elicit the anti-obesity, insulin sensitizing, and hepatoprotective functions in mice challenged with HFD. Treatment with TUDCA restored adipose SIRT1-mediated metabolic functions in clusterin-deficient mice. Molecular analyses revealed that SIRT1 and clusterin were both expressed and enriched in MERCs and acted together to regulate the protein and lipid compositions of the specialized subcellular microdomain, in turn modulating the crosstalk between mitochondrial and ER under different pathophysiological conditions.

In mammalian cells, ER is involved in the protein and lipid biosynthesis, whereas mitochondria are the essential organelles for oxidative phosphorylation and ATP production. The two organelles actively regulate each other's structure and function via MERCs, which play important roles in the coordination

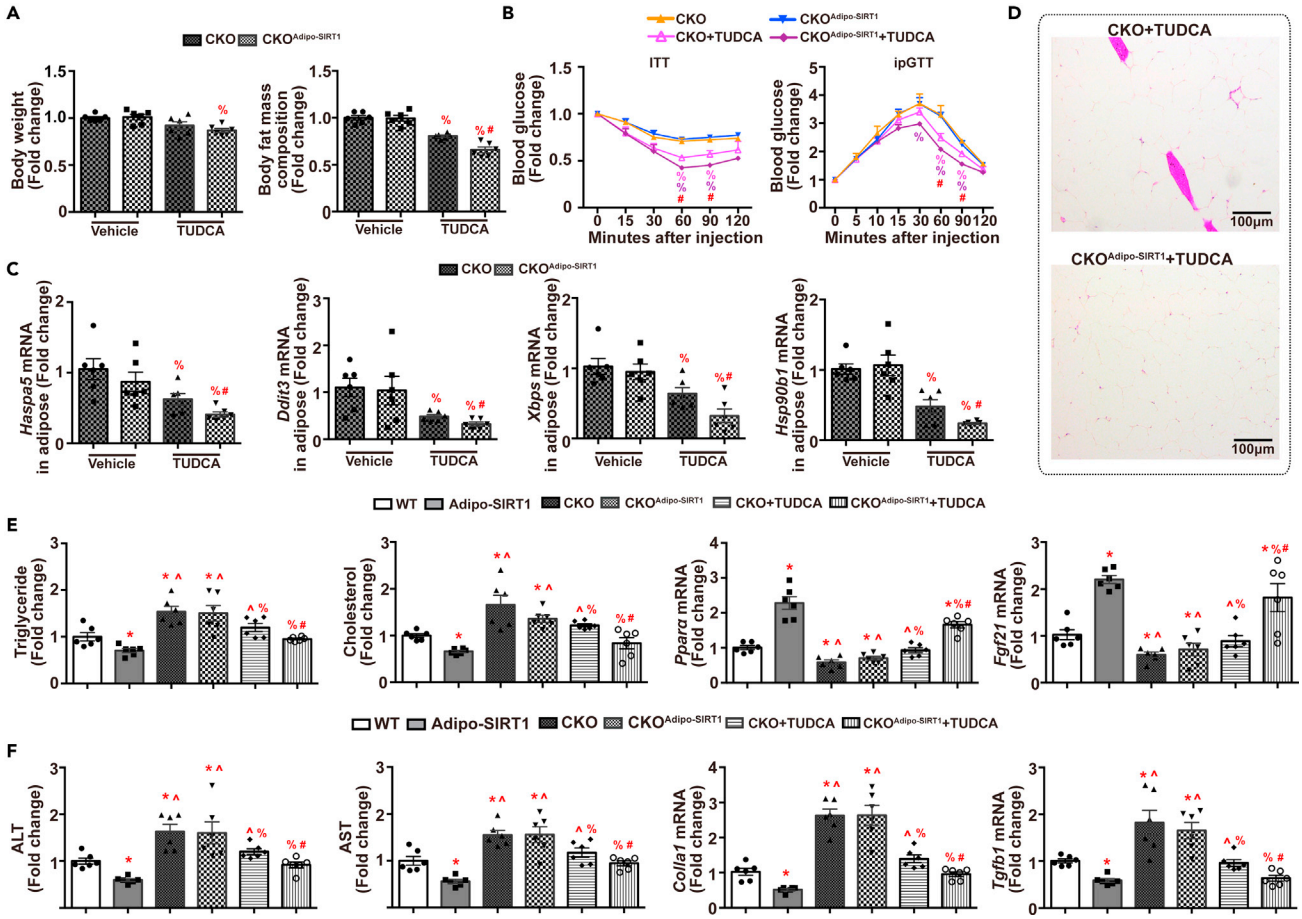

Figure 8. Treatment with TUDCA partially restores adipose SIRT1-mediated metabolic function in clusterin-deficient mice

CKO and CKO$^{Adipo-SIRT1}$ under HFD were administered with vehicle or TUDCA (300 mg/kg/day, i.p.) for six weeks. At the end of treatment, after starvation for 16-h, various metabolic parameters were examined before sacrificing the animals for analyzing the serum and tissue samples.

(A) Body weight (left) and fat mass composition (right) of CKO and CKO$^{Adipo-SIRT1}$ treated with vehicle or TUDCA were measured. Results are presented as fold changes versus those of CKO vehicle.

(B) ITT and ipGTT were performed in CKO and CKO$^{Adipo-SIRT1}$ treated with vehicle or TUDCA. Results are presented as fold changes versus time zero of each experimental group.

(C) QPCR was performed to measure the mRNA expression of genes involved in UPR^{ER} in epididymal adipose tissue. The 18S rRNA was detected as an internal control for normalization. Results are presented as fold changes versus those of CKO vehicle.

(D) H&E staining was performed on the sections of epididymal adipose tissue of CKO or CKO$^{Adipo-SIRT1}$ treated with TUDCA. Scale bar, 100 μm.

(E) The triglyceride and cholesterol contents (left) and mRNA expression levels of *Ppara* and *Fgf21* (right) in liver were measured for comparison. Results are presented as fold changes versus those of WT samples.

(F) The circulating levels of ALT and AST (left) as well as the hepatic mRNA expression of *Colla1* and *Tgfb1* (right) were measured for comparison. Results are presented as fold changes versus those of WT samples. Data are shown as means ± SEM.*, $p<0.05$, compared with WT; ^, $p<0.05$ compared with Adipo-SIRT1; %, $p<0.05$ compared with CKO vehicle control; #, $p<0.05$ compared with CKO treated with TUDCA. (n = 6, One or Two-way ANOVA)

of various cellular processes including calcium trafficking, lipid biogenesis, mitochondrial dynamics, mito/autophagy, inflammation, and metabolic signaling (Townsend et al., 2020). ER and mitochondria move closer to increase MERCs under stress conditions (Eisner et al., 2018). MERCs contain many signaling molecules/complexes involved in the regulation of energy metabolism, stress responses, calcium homeostasis, and redox balance (Scorrano et al., 2019; Csordás et al., 2018). Communications between ER and mitochondria via MERCs facilitate the transfer of lipids, ROS, calcium ions and other metabolites (Zung and Schuldiner, 2020). Our previous study showed that SIRT1 physically interacts with GRP75, HSP60, and VDAC, proteins that are involved in the formation of tethering complex between ER and mitochondria (Law et al., 2009). The present results demonstrated that SIRT1 was expressed and enriched in MERCs to regulate the protein and lipid contents, in turn stimulating UPR^{mt} and facilitating the mitochondria-ER interorganelle signaling. Overexpression of SIRT1 significantly increased the protein amounts of VDAC,

GRP75, IP3R, ERO1α, and NDUFS2 in MERCs of Adipo-SIRT1. The increased amount of IP3R-GRP75-VDAC tethering complex mediates ER release and mitochondrial uptake of calcium to stimulate oxidative metabolism (Cardenas et al., 2010). The augmented levels of ERO1α, an ER oxidoreductin, and NDUFS2, a core subunit of the mitochondrial ETC complex I, contribute to local ROS production in MERCs (Csordás et al., 2018), which may trigger mitohormesis and UPRmt, a stress response leading to the transcription of nuclear-encoded mitochondrial genes that promote protein homeostasis within the organelle (Bar-Ziv et al., 2020). Importantly, the effect of UPR^{mt} can be maintained long into adulthood ensuring increased resistance to mitochondrial perturbations, such as those caused by HFD (Moltedo et al., 2019). Treatment with MitoTEMPOL, a mitochondria-targeted antioxidant agent, largely abolished the UPR^{mt}-induced by adipose SIRT1. The data in the present study collectively suggest an innermost relationship between the induction of UPRmt and the prevention of hyper-activated ER stress signaling in healthy adipose tissues, or *vice versa*, i.e., the inhibition of UPRmt and the hyperactivation of ER stress signaling in those of dietary obese animals.

Clusterin is an extreme sensitive sensor of oxidative stress and regulated by HSF1, a transcriptional regulator of UPR^{mt} (Katiyar et al., 2020). Under stress conditions, GRP78 facilitates the retrotranslocation and redistribution of clusterin to promote cell survival (Li et al., 2013). Clusterin expression in adipose tissue of Adipo-SIRT1 was highly upregulated and different from that in the liver, possibly due to alterative initiation of transcription or distinct glycosylation (Garcia-Aranda et al., 2018). Clusterin protein was enriched in MERCs isolated from adipose tissue of Adipo-SIRT1 and participated in the regulation of ER stress sensors, such as PERK and IRE1. Overexpression of SIRT1 significantly increased the protein amount of PERK and IRE1 in MERCs isolated from adipose tissue of Adipo-SIRT1, but not in those of $CKO^{Adipo-SIRT1}$. The oligomerization of PERK, the PERK-eIF2α-ATF4-CHOP and IRE1-XBP signaling, as well as the ATF6 pathway of ER stress responses were all significantly enhanced in adipose tissue of CKO mice challenged with HFD and could not be inhibited by overexpression of adipose SIRT1. The crosstalks between mitochondria and ER depend on not only the protein tethering complex but also the lipid composition within the microdomains of MERCs (Rowland and Voeltz, 2012). MERCs are enriched with cholesterol and phospholipids. Mitochondrial and ER stresses can both be triggered by altered membrane lipid composition (Gao et al., 2020; Sasi et al., 2020; Silva-Palacios et al., 2020; Moltedo et al., 2019). Depletion of cholesterol increases the association of MERCs with mitochondria (Fujimoto et al., 2012). Excess cholesterol loading and increased lipid saturation trigger UPR by facilitating the membrane associations of PERK or IRE1, independent of unfolded protein stress (Kitai et al., 2013; Lee et al., 2020; Micoogullari et al., 2020; Volmer et al., 2013). While the increased clusterin provided a defense mechanism against proteotoxicity, it may also regulate the lipid composition in MERCs. The presence of higher amount of clusterin facilitated the rapid incorporation of ω-3 PUFAs as conjugated esters in adipose tissue, especially in MERCs, of Adipo-SIRT1. Compared to WT, there was a significantly reduced amount of cholesterol and a more rapid turnover of ω-3 PUFAs, in line with an increased expression and secretion of clusterin in adipose tissue of Adipo-SIRT1. Clusterin binds to PUFA-containing phospholipid binding proteins, such as synaptojanin (Hoshino and Sakane, 2021). However, the detailed mechanisms underlying clusterin-mediated ω-3 PUFAs incorporation and trafficking in MERCs remain to be characterized. Without clusterin, the esterification of ω-3 PUFAs was significantly inhibited leading to their accumulation as free forms in adipose tissue of CKO and $CKO^{Adipo-SIRT1}$. These observations suggest that the altered lipid composition in MERCs is responsible for the excessive activation of ER stress and UPR^{ER} in adipose tissue of CKO and $CKO^{Adipo-SIRT1}$, which further downregulate SIRT1 expression leading to more severe metabolic abnormalities and systemic insulin resistance. Thus, clusterin represents a unique signaling molecule mediating the stress response of SIRT1 in adipose tissue. By enhancing the incorporation of ω-3 PUFAs and the elimination of cholesterol, clusterin may modulate the activation and/or inactivation of IRE1 and PERK localized within the microdomains of MERCs (Cho et al., 2019).

The present study also suggested that clusterin played an important role in mediating the systemic metabolic functions of adipose SIRT1. Overexpression of SIRT1 not only enhanced the basal, but also fish oil-stimulated expression and secretion of clusterin from adipose tissue. One of the mechanisms underlying clusterin's actions was the formation of HDL particles enriched with ω-3 PUFAs from adipose tissue. MERCs were originally described as a site for phospholipid biosynthesis, lipoprotein assembly, and secretion (Vance, 1990). The ratio of unsaturated and saturated acyl chains affects membrane fluidity and thickness (Van Meer et al., 2008). Apart from its role in the esterification of ω-3 PUFAs, the presence of clusterin in MERCs may enhance the biogenesis of HDL particles from adipose tissue of Adipo-SIRT1. Increased

expression and secretion of clusterin and ApoA1 as well as the enhanced ABCA1 act synergistically to promote lipid efflux via HDL excretion from adipose tissue (Babashamsi et al., 2019; Zhang et al., 2019). Adipocytes play an important role in nascent HDL particle formation (Chung et al., 2011; Zhang et al., 2010). Significantly higher amounts of clusterin and ω-3 PUFAs were present in the HDL particles isolated from Adipo-SIRT1, which in turn elicited systemic insulin sensitizing, anti-inflammatory and hepatoprotective functions against MAFLD. The amount of conjugated ω-3 PUFAs significantly reduced in the liver whereas that of free ω-3 PUFAs significantly increased in adipose tissue of CKO. Despite the information, it is not clear how clusterin facilitates the esterification of ω-3 PUFAs in adipose tissue and subsequent packaging into HDL for systemic delivery. Nevertheless, the data suggest that ω-3 PUFAs are critically involved in mediating the anti-ER stress and hepatoprotective functions of adipose SIRT1.

Without clusterin, significantly reduced UPR^{mt} was associated with loss-of-protection against HFD-induced ER stress, which was largely attributed to the downregulation of SIRT1 expression in adipose tissue of CKOAdipo-SIRT1. Inhibition of IRE1, the most ancient ER stress sensor, significantly increased the mRNA levels of SIRT1 in adipose tissues of CKO and CKOAdipo-SIRT1. Although, at this stage, it is not known whether IRE1 directly, via its RNase activity, or indirectly, via other molecules such as microRNAs or human antigen R (HuR), to regulate the mRNA stability of human *SIRT1* and murine *Sirt1*. Although ω-3 PUFAs are well-known ER stress inhibitors, the present study demonstrated that they were ineffective in the restoration of SIRT1 expression and the metabolic functions of CKO and CKOAdipo-SIRT1, but involved in the induction of UPR^{mt} in adipose tissues of Adipo-SIRT1. More careful investigations are warranted to dissect the precise role of ω-3 PUFAs, as a whole or individual species, in modulating the mitochondrial and ER stress responses. Of great interest is that the mRNA transcripts of SIRT1 and other genes for UPR^{mt} were abundantly present in MERCs of adipose tissue. Moreover, MERCs contained other subsets of mRNA transcripts, such as those encoding various proteins for the biogenesis and assembly of plasma lipoprotein particles, which in turn contributes to systemic lipid metabolism and homeostasis (Anastasia et al., 2021). The composition and dynamic regulation of mRNA transcripts located at MERCs need to be further characterized.

In summary, selective overexpression of human SIRT1 in adipose tissue protected mice from HFD-induced metabolic abnormalities at least partly by upregulating clusterin, facilitating HDL biogenesis and delivery of esterified ω-3 PUFAs to other organs, including liver.

Limitation of the study

There are possible drawbacks of the model system studied. It remains unclear how SIRT1 and clusterin are regulated and cooperate to control the optimal lipid and protein compositions at MERCs in adipose tissue.

STAR★METHODS

Detailed methods are provided in the online version of this paper and include the following:

- KEY RESOURCES TABLE
- RESOURCE AVAILABILITY
  - Lead contact
  - Materials availability
  - Data and code availability
- EXPERIMENTAL MODEL AND SUBJECT DETAILS
  - Animals
- METHOD DETAILS
  - Metabolic evaluation
  - Histological examination
  - Lipoprotein fractionation
  - Mitochondrial isolation and ROS measurement
  - Mitochondrial respiration
  - Isolation of MERCs
  - Lipid analyses by GC-MS
  - Transmission electron microscopy (TEM)
  - Western blotting
  - Quantitative polymerase chain reactions (QPCR)
- QUANTIFICATION AND STATISTICAL ANALYSIS

SUPPLEMENTAL INFORMATION

Supplemental information can be found online at https://doi.org/10.1016/j.isci.2021.103709.

ACKNOWLEDGMENTS

This work was supported by the grants from Seeding Funds for Basic Research of the University of Hong Kong, the General Research Funds (17153016, 17124718, 17124420) and Collaborative Research Funds (C7037-17W) of Research Grant Council, the Areas of Excellence Scheme (AoE/M-707/18) of University Grants Committee, Hong Kong SAR; Basic Science Research Program of the National Research Foundation, Korea Ministry of Science and ICT (NRF-2017R1A2B3006406 and NRF-2020R1C1C1012729). Research in GB and AM laboratories is funded by Health Research Council of New Zealand (17/298) and Sir Charles Hercus Fellowship (17/058).

AUTHOR CONTRIBUTIONS

PZ, DK, and YZ performed the experiment; PZ, DK, YZ, and YW analyzed the data; PZ, DK, YZ, JHJ, and YW wrote the manuscript; GB and AM advised on the project and revised the manuscript; AX, IKL, AM, and YW designed the project and supervised the study. During the submission of this manuscript, Dr Alok Mitra passed away on July 2, 2021. His passion and rigor in science, cheerful friendship and courageous life will never be forgotten.

DECLARATION OF INTERESTS

The authors declare no competing interests.

Received: July 26, 2021
Revised: November 17, 2021
Accepted: December 24, 2021
Published: January 21, 2022

REFERENCES

Anastasia, I., Ilacqua, N., Raimondi, A., Lemieux, P., Ghandehari-Alavijeh, R., Faure, G., Mekhedov, S.L., Williams, K.J., Caicci, F., Valle, G., et al. (2021). Mitochondria-rough-er contacts in the liver regulate systemic lipid homeostasis. Cell Rep. *34*, 108873.

Anderson, N.S., and Haynes, C.M. (2020). Folding the mitochondrial upr into the integrated stress response. Trends Cell Biol. *30*, 428–439.

Avalli, A., and Contarini, G. (2005). Determination of phospholipids in dairy products by spe/hplc/elsd. J. Chromatogr. A *1071*, 185–190.

Babashamsi, M.M., Koukhaloo, S.Z., Halalkhor, S., Salimi, A., and Babashamsi, M. (2019). Abca1 and metabolic syndrome; a review of the abca1 role in hdl-vldl production, insulin-glucose homeostasis, inflammation and obesity. Diabetes Metab.Syndr. *13*, 1529–1534.

Bai, B., Liang, Y., Xu, C., Lee, M.Y., Xu, A., Wu, D., Vanhoutte, P.M., and Wang, Y. (2012). Cyclin-dependent kinase 5-mediated hyperphosphorylation of sirtuin-1 contributes to the development of endothelial senescence and atherosclerosis. Circulation *126*, 729–740.

Bar-Ziv, R., Bolas, T., and Dillin, A. (2020). Systemic effects of mitochondrial stress. EMBO Rep. *21*, e50094.

Bárcena, C., Mayoral, P., and Quirós, P.M. (2018). Mitohormesis, an antiaging paradigm. Int. Rev.Cell Mol. Biol. *340*, 35–77.

Basconcillo, L.S., and Mccarry, B.E. (2008). Comparison of three gc/ms methodologies for the analysis of fatty acids in sinorhizobium meliloti: development of a micro-scale, one-vial method. J. Chromatogr. B *871*, 22–31.

Bhattarai, K.R., Chaudhary, M., Kim, H.-R., and Chae, H.-J. (2020). Endoplasmic reticulum (er) stress response failure in diseases. Trends Cell Biol. *30*, 672–675.

Boutagy, N.E., Pyne, E., Rogers, G.W., Ali, M., Hulver, M.W., and Frisard, M.I. (2015). Isolation of mitochondria from minimal quantities of mouse skeletal muscle for high throughput microplate respiratory measurements. J. Vis.Exp. *105*, 53217.

Brousseau, T., Clavey, V., Bard, J., and Fruchart, J. (1993). Sequential ultracentrifugation micromethod for separation of serum lipoproteins and assays of lipids, apolipoproteins, and lipoprotein particles. Clin. Chem. *39*, 960–964.

Brown, M., Dainty, S., Strudwick, N., Mihai, A.D., Watson, J.N., Dendooven, R., Paton, A.W., Paton, J.C., and Schroder, M. (2020). Endoplasmic reticulum stress causes insulin resistance by inhibiting delivery of newly synthesized insulin receptors to the cell surface. Mol. Biol.Cell *31*, 2597–2629.

Cardenas, C., Miller, R.A., Smith, I., Bui, T., Molgo, J., Muller, M., Vais, H., Cheung, K.H., Yang, J., Parker, I., et al. (2010). Essential regulation of cell bioenergetics by constitutive insp3 receptor ca2+ transfer to mitochondria. Cell *142*, 270–283.

Cheng, H., Gang, X., He, G., Liu, Y., Wang, Y., Zhao, X., and Wang, G. (2020). The molecular mechanisms underlying mitochondria-associated endoplasmic reticulum membrane-induced insulin resistance. Front. Endocrinol. *11*, 592129.

Cho, H., Stanzione, F., Oak, A., Kim, G.H., Yerneni, S., Qi, L., Sum, A.K., and Chan, C. (2019). Intrinsic structural features of the human ire1alpha transmembrane domain sense membrane lipid saturation. Cell Rep. *27*, 307–320 e5.

Chung, S., Sawyer, J.K., Gebre, A.K., Maeda, N., and Parks, J.S. (2011). Adipose tissue atp binding cassette transporter a1 contributes to high-density lipoprotein biogenesis in vivo. Circulation *124*, 1663–1672.

Csordás, G., Weaver, D., and Hajnóczky, G. (2018). Endoplasmic reticulum–mitochondrial contactology: structure and signaling functions. Trends Cell Biol. *28*, 523–540.

Eisner, V., Picard, M., and Hajnoczky, G. (2018). Mitochondrial dynamics in adaptive and maladaptive cellular stress responses. Nat.Cell Biol. *20*, 755–765.

English, A.M., Schuler, M.H., Xiao, T., Kornmann, B., Shaw, J.M., and Hughes, A.L. (2020). Er-mitochondria contacts promote mitochondrial-derived compartment biogenesis. J.Cell Biol. *219*, e202002144.

Farghali, H., Kemelo, M.K., and Canova, N.K. (2019). Sirt1 modulators in experimentally

induced liver injury. Oxid. Med.CellLongev. *2019*, 8765954.

Feige, J.N., Lagouge, M., Canto, C., Strehle, A., Houten, S.M., Milne, J.C., Lambert, P.D., Mataki, C., Elliott, P.J., and Auwerx, J. (2008). Specific sirt1 activation mimics low energy levels and protects against diet-induced metabolic disorders by enhancing fat oxidation. Cell Metab. *8*, 347–358.

Fujimoto, M., Hayashi, T., and Su, T.P. (2012). The role of cholesterol in the association of endoplasmic reticulum membranes with mitochondria. Biochem.Biophys. Res. Commun. *417*, 635–639.

Gao, P., Yan, Z., and Zhu, Z. (2020). Mitochondria-associated endoplasmic reticulum membranes in cardiovascular diseases. Front.Cell Dev. Biol. *8*, 604240.

Garcia-Aranda, M., Serrano, A., and Redondo, M. (2018). Regulation of clusterin gene expression. Curr.Protein Pept. Sci. *19*, 612–622.

Gregor, M.F., Yang, L., Fabbrini, E., Mohammed, B.S., Eagon, J.C., Hotamisligil, G.S., and Klein, S. (2009). Endoplasmic reticulum stress is reduced in tissues of obese subjects after weight loss. Diabetes *58*, 693–700.

Guo, Y., Xu, C., Man, A.W.C., Bai, B., Luo, C., Huang, Y., Xu, A., Vanhoutte, P.M., and Wang, Y. (2019). Endothelial sirt1 prevents age-induced impairment of vasodilator responses by enhancing the expression and activity of soluble guanylyl cyclase in smooth muscle cells. Cardiovasc. Res. *115*, 678–690.

Hetz, C., Zhang, K., and Kaufman, R.J. (2020). Mechanisms, regulation and functions of the unfolded protein response. Nat. Rev. Mol.Cell Biol. *21*, 421–438.

Hoofnagle, A.N., Wu, M., Gosmanova, A.K., Becker, J.O., Wijsman, E.M., Brunzell, J.D., Kahn, S.E., Knopp, R.H., Lyons, T.J., and Heinecke, J.W. (2010). Low clusterin levels in high-density lipoprotein associate with insulin resistance, obesity, and dyslipoproteinemia. Arterioscler Thromb.Vasc. Biol. *30*, 2528–2534.

Hoshino, F., and Sakane, F. (2021). Polyunsaturated fatty acid-containing phosphatidic acid interacts with synaptojanin-1 and enhances its phosphoinositide d-4-phosphatase activity. FASEB J. *35*. https://doi.org/10.1096/fasebj.2021.35.S1.01910.

Hui, X., Zhang, M., Gu, P., Li, K., Gao, Y., Wu, D., Wang, Y., and Xu, A. (2017). Adipocyte sirt1 controls systemic insulin sensitivity by modulating macrophages in adipose tissue. EMBO Rep. *18*, 645–657.

Katiyar, A., Fujimoto, M., Tan, K., Kurashima, A., Srivastava, P., Okada, M., Takii, R., and Nakai, A. (2020). Hsf1 is required for induction of mitochondrial chaperones during the mitochondrial unfolded protein response. FEBS Open Bio. *10*, 1135–1148.

Kitai, Y., Ariyama, H., Kono, N., Oikawa, D., Iwawaki, T., and Arai, H. (2013). Membrane lipid saturation activates ire1alpha without inducing clustering. Genes Cells *18*, 798–809.

Kwon, M.J., Ju, T.J., Heo, J.Y., Kim, Y.W., Kim, J.Y., Won, K.C., Kim, J.R., Bae, Y.K., Park, I.S., Min, B.H., et al. (2014). Deficiency of clusterin exacerbates high-fat diet-induced insulin resistance in male mice. Endocrinology *155*, 2089–2101.

Labbadia, J., Brielmann, R.M., Neto, M.F., Lin, Y.F., Haynes, C.M., and Morimoto, R.I. (2017). Mitochondrial stress restores the heat shock response and prevents proteostasis collapse during aging. Cell Rep. *21*, 1481–1494.

Labunskyy, V.M., Gerashchenko, M.V., Delaney, J.R., Kaya, A., Kennedy, B.K., Kaeberlein, M., and Gladyshev, V.N. (2014). Lifespan extension conferred by endoplasmic reticulum secretory pathway deficiency requires induction of the unfolded protein response. PLoS Genet. *10*, e1004019.

Lam, J., Katti, P., Biete, M., Mungai, M., Ashshareef, S., Neikirk, K., Garza Lopez, E., Vue, Z., Christensen, T.A., Beasley, H.K., et al. (2021). A universal approach to analyzing transmission electron microscopy with imagej. Cells *10*, 2177.

Law, I.K., Liu, L., Xu, A., Lam, K.S., Vanhoutte, P.M., Che, C.M., Leung, P.T., and Wang, Y. (2009). Identification and characterization of proteins interacting with sirt1 and sirt3: implications in the anti-aging and metabolic effects of sirtuins. Proteomics *9*, 2444–2456.

Lee, S.M., Lee, S.H., Jung, Y., Lee, Y., Yoon, J.H., Choi, J.Y., Hwang, C.Y., Son, Y.H., Park, S.S., Hwang, G.S., et al. (2020). Fabp3-mediated membrane lipid saturation alters fluidity and induces er stress in skeletal muscle with aging. Nat. Commun. *11*, 5661.

Lepretti, M., Martucciello, S., Burgos Aceves, M.A., Putti, R., and Lionetti, L. (2018). Omega-3 fatty acids and insulin resistance: focus on the regulation of mitochondria and endoplasmic reticulum stress. Nutrients *10*, 350.

Li, N., Zoubeidi, A., Beraldi, E., and Gleave, M.E. (2013). Grp78 regulates clusterin stability, retrotranslocation and mitochondrial localization under er stress in prostate cancer. Oncogene *32*, 1933–1942.

Melber, A., and Haynes, C.M. (2018). Upr(mt) regulation and output: a stress response mediated by mitochondrial-nuclear communication. Cell Res. *28*, 281–295.

Metcalf, M.G., Higuchi-Sanabria, R., Garcia, G., Tsui, C.K., and Dillin, A. (2020). Beyond the cell factory: homeostatic regulation of and by the upr(er). Sci. Adv. *6*, eabb9614.

Micoogullari, Y., Basu, S.S., Ang, J., Weisshaar, N., Schmitt, N.D., Abdelmoula, W.M., Lopez, B., Agar, J.N., Agar, N., and Hanna, J. (2020). Dysregulation of very-long-chain fatty acid metabolism causes membrane saturation and induction of the unfolded protein response. Mol. Biol.Cell *31*, 7–17.

Moltedo, O., Remondelli, P., and Amodio, G. (2019). The mitochondria-endoplasmic reticulum contacts and their critical role in aging and age-associated diseases. Front.Cell Dev. Biol. *7*, 172.

Montesinos, J., and Area-Gomez, E. (2020). Isolation of mitochondria-associated er membranes. Methods Cell Biol. *155*, 33–44.

Okada, L., Oliveira, C.P., Stefano, J.T., Nogueira, M.A., Silva, I., Cordeiro, F.B., Alves, V.a.F., Torrinhas, R.S., Carrilho, F.J., Puri, P., and Waitzberg, D.L. (2018). Omega-3 pufa modulate lipogenesis, er stress, and mitochondrial dysfunction markers in nash - proteomic and lipidomic insight. Clin.Nutr. *37*, 1474–1484.

Pardo, P.S., and Boriek, A.M. (2020). Sirt1 regulation in ageing and obesity. Mech. Ageing Dev. *188*, 111249.

Park, S., Mathis, K.W., and Lee, I.K. (2014). The physiological roles of apolipoprotein j/clusterin in metabolic and cardiovascular diseases. Rev. Endocr.Metab.Disord. *15*, 45–53.

Quirós, P.M., Mottis, A., and Auwerx, J. (2016). Mitonuclear communication in homeostasis and stress. Nat. Rev. Mol.Cell Biol. *17*, 213–226.

Rieusset, J. (2018). The role of endoplasmic reticulum-mitochondria contact sites in the control of glucose homeostasis: an update. Cell Death Dis. *9*, 1–12.

Ristow, M., and Schmeisser, S. (2011). Extending life span by increasing oxidative stress. Free Radic. Biol. Med. *51*, 327–336.

Rogers, G.W., Brand, M.D., Petrosyan, S., Ashok, D., Elorza, A.A., Ferrick, D.A., and Murphy, A.N. (2011). High throughput microplate respiratory measurements using minimal quantities of isolated mitochondria. PloS One *6*, e21746.

Rowland, A.A., and Voeltz, G.K. (2012). Endoplasmic reticulum-mitochondria contacts: function of the junction. Nat. Rev. Mol.Cell Biol. *13*, 607–625.

Rull, A., Martínez-Bujidos, M., Pérez-Cuellar, M., Pérez, A., Ordóñez-Llanos, J., and Sánchez-Quesada, J.L. (2015). Increased concentration of clusterin/apolipoprotein j (apoj) in hyperlipemic serum is paradoxically associated with decreased apoj content in lipoproteins. Atherosclerosis *241*, 463–470.

Sasi, U.S.S., Ganapathy, S., Palayyan, S.R., and Gopal, R.K. (2020). Mitochondria associated membranes (mams): emerging drug targets for diabetes. Curr. Med. Chem. *27*, 3362–3385.

Schreiner, B., and Ankarcrona, M. (2017). Isolation of mitochondria-associated membranes (mam) from mouse brain tissue. Methods Mol. Biol. *1567*, 53–68.

Scorrano, L., De Matteis, M.A., Emr, S., Giordano, F., Hajnóczky, G., Kornmann, B., Lackner, L.L., Levine, T.P., Pellegrini, L., Reinisch, K., et al. (2019). Coming together to define membrane contact sites. Nat. Commun. *10*, 1287.

Silva-Palacios, A., Zazueta, C., and Pedraza-Chaverri, J. (2020). Er membranes associated with mitochondria: possible therapeutic targets in heart-associated diseases. Pharmacol.Res. *156*, 104758.

Strycharz, J., Rygielska, Z., Swiderska, E., Drzewoski, J., Szemraj, J., Szmigiero, L., and Sliwinska, A. (2018). Sirt1 as a therapeutic target in diabetic complications. Curr. Med. Chem. *25*, 1002–1035.

Strzyz, P. (2019). Er stress boosts respiration. Nat. Rev. Mol.Cell Biol. *20*, 453.

Townsend, L.K., Brunetta, H.S., and Mori, M.a.S. (2020). Mitochondria-associated er membranes in glucose homeostasis and insulin resistance. Am. J. Physiol. Endocrinol.Metab. *319*, E1053–E1060.

Trnka, J., Blaikie, F.H., Logan, A., Smith, R.A., and Murphy, M.P. (2009). Antioxidant properties of mitotempol and its hydroxylamine. Free Radic. Res. *43*, 4–12.

Tubbs, E., Chanon, S., Robert, M., Bendridi, N., Bidaux, G., Chauvin, M.A., Ji-Cao, J., Durand, C., Gauvrit-Ramette, D., Vidal, H., et al. (2018). Disruption of mitochondria-associated endoplasmic reticulum membrane (mam) integrity contributes to muscle insulin resistance in mice and humans. Diabetes *67*, 636–650.

Van Meer, G., Voelker, D.R., and Feigenson, G.W. (2008). Membrane lipids: where they are and how they behave. Nat. Rev. Mol.Cell Biol. *9*, 112–124.

Vance, J.E. (1990). Phospholipid synthesis in a membrane fraction associated with mitochondria. J. Biol. Chem. *265*, 7248–7256.

Volmer, R., Van Der Ploeg, K., and Ron, D. (2013). Membrane lipid saturation activates endoplasmic reticulum unfolded protein response transducers through their transmembrane domains. Proc. Natl. Acad. Sci. U S A. *110*, 4628–4633.

Wang, Y., Xu, C., Liang, Y., and Vanhoutte, P.M. (2012). Sirt1 in metabolic syndrome: where to target matters. Pharmacol.Ther. *136*, 305–318.

Wieckowski, M.R., Giorgi, C., Lebiedzinska, M., Duszynski, J., and Pinton, P. (2009). Isolation of mitochondria-associated membranes and mitochondria from animal tissues and cells. Nat. Protoc. *4*, 1582–1590.

Wilson, M.R., and Zoubeidi, A. (2017). Clusterin as a therapeutic target. Expert Opin.Ther. Targets *21*, 201–213.

Xu, C., Bai, B., Fan, P., Cai, Y., Huang, B., Law, I.K., Liu, L., Xu, A., Tung, C., Li, X., et al. (2013). Selective overexpression of human sirt1 in adipose tissue enhances energy homeostasis and prevents the deterioration of insulin sensitivity with ageing in mice. Am. J. Transl. Res. *5*, 412–426.

Xu, C., Cai, Y., Fan, P., Bai, B., Chen, J., Deng, H.B., Che, C.M., Xu, A., Vanhoutte, P.M., and Wang, Y. (2015). Calorie restriction prevents metabolic aging caused by abnormal sirt1 function in adipose tissues. Diabetes *64*, 1576–1590.

Zatterale, F., Longo, M., Naderi, J., Raciti, G.A., Desiderio, A., Miele, C., and Beguinot, F. (2019). Chronic adipose tissue inflammation linking obesity to insulin resistance and type 2 diabetes. Front. Physiol. *10*, 1607.

Zhang, P., Konja, D., Zhang, Y., and Wang, Y. (2021). Communications between mitochondria and endoplasmic reticulum in the regulation of metabolic homeostasis. Cells *10*, 2195.

Zhang, T., Chen, J., Tang, X., Luo, Q., Xu, D., and Yu, B. (2019). Interaction between adipocytes and high-density lipoprotein:New insights into the mechanism of obesity-induced dyslipidemia and atherosclerosis. Lipids Health Dis. *18*, 223.

Zhang, Y., Mcgillicuddy, F.C., Hinkle, C.C., O'neill, S., Glick, J.M., Rothblat, G.H., and Reilly, M.P. (2010). Adipocyte modulation of high-density lipoprotein cholesterol. Circulation *121*, 1347–1355.

Zu, Y., Liu, L., Lee, M.Y., Xu, C., Liang, Y., Man, R.Y., Vanhoutte, P.M., and Wang, Y. (2010). Sirt1 promotes proliferation and prevents senescence through targeting lkb1 in primary porcine aortic endothelial cells. Circ. Res. *106*, 1384–1393.

Zung, N., and Schuldiner, M. (2020). New horizons in mitochondrial contact site research. Biol. Chem. *401*, 793–809.

STAR★METHODS

KEY RESOURCES TABLE

REAGENT or RESOURCE	SOURCE	IDENTIFIER
Antibodies		
Anti-ApoA1 antibody	Abcam	RRID: AB_2892531
Anti-ATF6 antibody	Invitrogen	RRID: AB_11156398
Anti-β-Actin antibody	Sigma-Aldrich	RRID: AB_476743
Anti-Clusterin α chain antibody	Abcam	RRID: AB_2892532
Anti-Clusterin β chain antibody	Abcam	RRID: AB_2892533
Anti-eIF2α antibody	CST	RRID: AB_10692650
Anti-ERO1α antibody	Invitrogen	RRID: AB_2716886
Anti-GRP78 antibody	Abcam	RRID: AB_2119834
Anti-IP3R antibody	Abcam	RRID: AB_305124
Anti-IRE1 antibody	CST	RRID: AB_823545
Anti-Mitofusin-2 antibody	CST	RRID: AB_2716838
Anti-NDUFS2 antibody	Abcam	RRID: AB_2892535
Anti-PERK antibody	CST	RRID: AB_2095847
Anti-p-eIF2α (Ser51) antibody	CST	RRID: AB_390740
Anti-p-IRE1 (Ser724) antibody	NOVUS	RRID: AB_10145203
Anti-SIRT1 antibody	EMD Millipore	RRID: AB_11214517
Anti-α-Tubulin antibody	Sigma-Aldrich	RRID: AB_477579
Anti-VDAC antibody	Abcam	RRID: AB_2687466
Anti-XBPs antibody	Abcam	RRID: AB_778939
Goat anti-rabbit IgG-HRP	CST	RRID: AB_2099233
Goat anti-mouse IgG-HRP	CST	RRID: AB_330924
Chemicals		
Fish oil	Drapac	B1 2030010
Mitotempol (2,2,6,6-tetramethyl-4-[[5-(triphenylphosphonio)pentyl]oxy]-1-piperidinyloxy, monobromide)	Cayman Chemical	18796; CAS No. 1101113-39-6
TUDCA (3α,7β-Dihydroxy-5β-cholan-24-oic acid N-(2-sulfoethyl)amide, Tauroursodeoxycholic acid sodium salt)	Sigma-Aldrich	T0266; CAS No. 35807-85-3
4μ8c (7-Hydroxy-4-methyl-2-oxo-2H-1-benzopyran-8-carboxaldehyde)	Selleck Chemicals	S7272; CAS No.14003-96-4
MKC8866 (7-hydroxy-6-methoxy-4-methyl-3-(2-morpholin-4-yl-2-oxoethyl)-2-oxochromene-8-carbaldehyde)	Selleck Chemicals	S8875; CAS No.1338934-59-0
STF083010 (N-[(2-hydroxynaphthalen-1-yl) methylidene]thiophene-2-sulfonamide)	Selleck Chemicals	S7771; CAS No.307543-71-1
KIRA6 (1-[4-(8-amino-3-tert-butylimidazo[1,5-a] pyrazin-1-yl)naphthalen-1-yl]-3-[3-(trifluoromethyl) phenyl]urea)	Selleck Chemicals	S8658; CAS No.1589527-65-0
Oil Red O (1-[[4-[(2,5-dimethylphenyl)diazenyl]-2,5-dimethylphenyl]diazenyl]naphthalen-2-ol)	Sigma-Aldrich	O0625; CAS No.1320-06-5

(*Continued on next page*)

Continued

REAGENT or RESOURCE	SOURCE	IDENTIFIER
ADP (sodium;[[(2S)-2-[(1R)-1-(6-aminopurin-9-yl)-2-oxoethoxy]-3-oxopropoxy]-hydroxyphosphoryl] hydrogen phosphate)	Sigma-Aldrich	A2754; CAS No. 20398-34-9
Oligomycin ((1S,4E,5'R,6R,6'R,7S,8R,10S,11S,12R,14S,15R,16S,18E,20E,22S,25R,27S,28R,29S)-22-ethyl-7,11,14,15-tetrahydroxy-6'-[(2S)-2-hydroxypropyl]-5',6,8,10,12,14,16,28,29-nonamethylspiro[2,26-dioxabicyclo[23.3.1]nonacosa-4,18,20-triene-27,2'-oxane]-3,9,13-trione)	Sigma-Aldrich	495455; CAS No. 1404-19-9
FCCP (2-[[4-(trifluoromethoxy)phenyl]hydrazinylidene] propanedinitrile)	Sigma-Aldrich	C2920; CAS No. 370-86-5
Rotenone ((1S,6R,13S)-16,17-dimethoxy-6-prop-1-en-2-yl-2,7,20-trioxapentacyclo[11.8.0.03,11.04,8.014,19]henicosa-3(11),4(8),9,14,16,18-hexaen-12-one)	Sigma-Aldrich	R8875; CAS No. 83-79-4
Antimycin A ([(2R,3S,6S,7R,8R)-3-[(3-formamido-2-hydroxybenzoyl)amino]-8-hexyl-2,6-dimethyl-4,9-dioxo-1,5-dioxonan-7-yl] 3-methylbutanoate)	Sigma-Aldrich	A8674; CAS No. 1397-94-0
Methyl nonadecanoate	Sigma-Aldrich	N5733; CAS No. 1731-94-8
Critical commercial assays		
LiquiColor Triglycerides assay kit	Stanbio Laboratory	2200-430
LiquiColor Cholesterol assay kit	Stanbio Laboratory	1010-430
Mouse insulin assay ELISA kit	Immunodiagnostics	33270
Stanbio Laboratory ALT/SGPT Liqui-UV Test	Stanbio Laboratory	2930-430
Stanbio Laboratory AST/SGOT Liqui-UV Test	Stanbio Laboratory	2920-430
MitoSOX™ Red	Thermo Fisher Scientific	M36008
Deposited data		
Raw and analyzed data	This paper	Mendeley Data: https://doi.org/10.17632/x95xs73w9n.1
Experimental models: Organisms/strains		
Mouse/C57BL/6J	CCMR, HKU https://www.lau.hku.hk/	NA
Mouse/Adipo-SIRT1	CCMR, HKU https://www.lau.hku.hk/	NA
Mouse/CKO	CCMR, HKU https://www.lau.hku.hk/	NA
Mouse/CKO$^{Adipo\text{-}SIRT1}$	CCMR, HKU https://www.lau.hku.hk/	NA
Oligonucleotides		
Primers for genotyping and QPCR	This paper	N/A
Software and algorithms		
ImageJ	NIH	https://imagej.nih.gov/ij/
GraphPad Prism version 8.0.2	GraphPad	https://www.graphpad.com/

RESOURCE AVAILABILITY

Lead contact

Further information and requests for resources and reagents should be directed to and will be fulfilled by the lead contact, Yu Wang (yuwanghk@hku.hk).

Materials availability

This study did not generate new unique reagents.

Data and code availability

- The raw and processed data have been deposited to Mendeley Data: https://doi.org/10.17632/x95xs73w9n.1 and are publicly available as of the date of publication.
- Any additional information required to reanalyze the data reported in this paper is available from the lead contact upon request.

EXPERIMENTAL MODEL AND SUBJECT DETAILS

Animals

All procedures were approved by the Committee on the Use of Live Animals for Teaching and Research (CULATR 4951-19) of the University of Hong Kong and carried out in accordance with the criteria outlined in the Guide for the Care and Use of Laboratory Animals prepared by the National Academy of Sciences and published by the National Institutes of Health (NIH). Mice with selective overexpression of human SIRT1 in adipose tissues (Adipo-SIRT1) were generated by our own lab (Xu et al., 2013, 2015). The clusterin knockout mice (CKO) were established and characterized in a previous study (Kwon et al., 2014). The $CKO^{Adipo-SIRT1}$ mice were generated by crossbreeding Adipo-SIRT1 with CKO. All animals were maintained in a C57BL/6J background and housed in a room under controlled temperature (23 ± 1°C) and 12 h light-dark cycles, with free access to water and standard chow (LabDiet 5053; LabDiet, Purina Mills, Richmond, IN, USA). Genotyping PCR was performed using primers listed in Table S3. Male animals were used for the present study and randomly assigned to each experimental group. Starting from the age of five weeks, mice were fed with a HFD (D12451; Research Diet, New Brunswick, NJ, USA). For short-term treatment, eight-week-old mice under STC were given a single dose (by oral gavage) of 0.2 mL fish oil (Drapac, Auckland, New Zealand) containing ~18% EPA and ~12% DHA. Before and at three, six, or nine hours after oral gavage, serum, and tissue samples were collected for analyses. Mice under HFD were also subjected to a one-week treatment with mitotempol (Cayman Chemical, MI, USA; 1 mg/kg/day, i.p.), TUDCA (Sigma-Aldrich, MO, USA; 300 mg/kg/day, i.p.) or a mixture of IRE1 inhibitors (Selleck, TX, USA) containing 4μ8c (10 mg/kg/day, i.p.), MKC8866 (20 mg/kg/day, i.p.), STF083010 (30 mg/kg/day, i.p.) and KIRA6 (5 mg/kg/day, i.p.). For long-term treatment, mice under HFD were administered with vehicle or TUDCA (300 mg/kg/day, i.p.) for six weeks, starting from the age of 11 weeks.

METHOD DETAILS

Metabolic evaluation

Body weight was recorded between 9 and 10 AM after overnight starvation. Blood glucose was monitored by tail nicking using an Accu-Check Advantage II Glucometer (Roche Diagnostics, Mannheim, Germany). The body fat mass composition was assessed in conscious and unanesthetized mice using a BruckerMinispec body composition analyzer (Bruker Optics Inc., Woodlands, TX, USA). For ITT, mice were starved for four hours and then administered with insulin (1 IU/kg body weight, i.p). For ipGTT, overnight (16 h) fasted mice were injected with glucose (1 g/kg body weight, i.p). Blood glucose was measured in samples obtained from the tail vein at different time points as indicated (Xu et al., 2015). Circulating levels and tissue contents of triglyceride and total cholesterol were analyzed using the LiquiColor Triglycerides and Stanbio Cholesterol assay kits (Catalogue No 2200-430 and 1010-430, respectively; Stanbio Laboratory, Boerne, TX, USA). The concentration of serum insulin was quantified using a commercial ELISA kit (Catalogue No 33270; Immunodiagnostics, Hong Kong, China). Serum levels of ALT and AST were analyzed using the commercial kits (Catalogue No 2930-430 and 2920-430, respectively) from Stanbio Laboratory. VO_2, VCO_2, RER and energy expenditure were measured by indirect calorimetry using a six-chamber open-circuit Oxymax/CLAMS Comprehensive Lab Animal Monitoring System (Columbus Instruments, Columbus, OH, USA) (Xu et al., 2015). All mice were acclimatized to the cage for 48 h before recording the parameters from a three-day feeding course.

Histological examination

Tissues were cut into small pieces and fixed in 10% neutral buffered formalin solution for 48 h before transferring to 75% ethanol for long-term storage at 4°C. The paraffin blocks were prepared for sectioning at 5 μm thickness. The tissue sections were stained with H&E for examination. The size of adipocytes was

measured randomly from ten fields and calculated as average cross-sectional area using the ImageJ software.

(Version 1.51, NIH, USA). For evaluation of lipid accumulation, frozen tissues embedded in Tissue-Tek OCT compound (Sakura® Finetek, CA, USA) were sectioned at 10 μm thickness and stained with Oil Red O (Sigma-Aldrich). All images were examined and captured using an Olympus biological microscope BX41, equipped with a DP72 color digital camera (Olympus, Tokyo, Japan).

Lipoprotein fractionation

The serum samples were fractionated on a potassium bromide (KBr) density gradient to isolate the HDL particles by ultracentrifugation (Brousseau et al., 1993). Briefly, an aliquot of 400 μL serum was overlaid on 600 μL of the KBr solution (d = 1.006 g/mL) and centrifuged for two hours at 45,000 g, 15°C using a TLA12.0 rotor (Beckman, IN, USA). The density was adjusted to 1.21 for the bottom fraction before ultracentrifugation for another three hours at 45,000 g, 15°C. The 400 μL top layer containing HDL particles were collected. The buffer in the HDL fractions was replaced with phosphate buffered saline (PBS) by centrifugation in a 3K MWCO Pierce^{TM} Protein Concentrator (Thermo Fisher Scientific, MA, USA). All HDL samples were stored at −80°C for subsequent analyses.

Mitochondrial isolation and ROS measurement

Mitochondria were isolated from epididymal adipose tissue for measuring the ROS levels (Rogers et al., 2011; Boutagy et al., 2015). Briefly, 200 mg tissue was homogenized in one ml mitochondria isolation buffer (MIB; 200 mM sucrose, 1 mM EGTA, 10 mM Tris/MOPS, pH 7.4) using a glass PTFE homogenizer (Sartorius, Göttingen, Germany) chilled on ice bath. The homogenate was centrifuged at 600 g for 10 min at 4°C. The supernatant was then centrifuged at 10,000 g for 10 min at 4°C to collect the crude mitochondrial pellet (Figure S2). Mitochondrial ROS were measured using the MitoSOX™ Red (Thermo Fisher Scientific, MA, USA) according to the manufacturer's instructions. Briefly, mitochondria test buffer (230 mM KCl, 20 mM KH_2PO_4, 8 mM $MgCl_2$, 40 mM HEPES, 100 μM EGTA, 5 μM MitoSOX™) supplemented with 3 mM ATP, 5 mM glutamate and 5 mM malate was incubated in a 96-well plate (Nunc, Roskilde, Denmark) at 37°C with or without inhibitors. After incubation, 10 μg mitochondria were added and fluorescence quantified immediately with a CLARIOstar microplate reader (BMG LABTECH, Ortenberg, Germany) at an excitation/emission wavelength of 510/580nm over 10 min.

Mitochondrial respiration

The experiment was performed on a Seahorse XFe24 Analyzer (Agilent, CA, USA). Briefly, one ml XFe24 calibration buffer was added to the wells of XFe24 sensor cartridge for overnight incubation at 37°C in a non-CO_2 incubator. Mitochondria assay solution (MAS; pH 7.4) containing 70 mM sucrose, 220 mM mannitol, 5 mM KH_2PO4, 5 mM $MgCl_2$ and 2 mM HEPES with or without 0.2% fatty acid-free bovine serum albumin was freshly prepared with supplementation of mitochondria complex I substrates, pyruvate (10 mM) and malate (5 mM). The XFe drugs were diluted to desired concentrations [adenosine diphosphate (ADP), 50 mM; oligomycin, 50 μM; trifluoromethoxy carbonylcyanide phenylhydrazone (FCCP), 50 μM; rotenone/antimycin A cocktail, 20 μM/100 μM] and injected as follows: port A, ADP (22 μL); port B, oligomycin (24 μL); port C, FCCP (26 μL); and port D, rotenone/antimycin A (28 μL). The mitochondria (15 μg) were re-suspended in the MAS with pyruvate/malate and loaded to each wells of the Seahorse microplate for data collection.

Isolation of MERCs

MERCs were purified from the crude mitochondria as described with modifications (Vance, 1990; Schreiner and Ankarcrona, 2017; Wieckowski et al., 2009; Montesinos and Area-Gomez, 2020). In brief, the crude mitochondria were re-suspended in mitochondria resuspension buffer containing 225 mM mannitol, 25 mM HEPES and 1 mM EGTA (pH 7.4) and then overlaid on a 30% Percoll medium, followed by ultracentrifugation for 30 min at 95,000 g, 4°C with a TLA12.0 rotor. MERCs, visible as the white bands located in the middle layer, were collected and diluted ten times with the above buffer and then centrifuged for 10 min at 6300 g, 4°C to precipitate the mitochondrial remnants. The supernatant was further centrifuged for one hour at 100,000 g, 4°C to collect the pellet of MERCs for subsequent analyses. The final yields were calculated by measuring the protein contents in MERCs and expressed as per gram of tissue used for isolation.

The other portion of the tissue homogenates was used to obtain ER and cytosol samples for analyzing the resident proteins and validating the fractionation protocol (Figure S2).

Lipid analyses by GC-MS

Liver or adipose tissue (five mg), HDL fractions (10 μg) or MERCs (5 μg) were mixed with 500 μL CHCl3: MeOH (2:1, v/v). Twenty-five μg of methyl nonadecanoate (C19:0; N5733, Sigma Aldrich) was added into each sample as an internal standard. After homogenization, the chloroform phase was separated by centrifugation at 3000 rpm for 15 min and dried under a nitrogen stream. For solid phase extraction, the total lipids of MERCs were applied to a silica bond column (Catalogue No 97728-U, Sigma-Aldrich, MO, USA). After conditioning with hexane, the neutral lipids were eluted with 0.5 mL of hexane-diethylether (8:2, v/v) and then 0.5 mL of hexane-diethylether (1:1, v/v). The phospholipids were eluted with 0.5 mL of methanol and then 0.5 mL of chloroform-methanol-water (3:5:2, v/v/v). The recovered fractions were dried under a gentle stream of nitrogen for GC-MS analysis (Avalli and Contarini, 2005). Saponification was performed to evaluate the conjugated (esterified) fatty acids (Basconcillo and Mccarry, 2008). Briefly, 500 μL of KOH-MeOH (10%, w/v) was added to the dried lipids for a two-hour incubation at 80°C. After neutralization with 200 μL of 6 M hydrochloric acid, the lipids were extracted twice with 500 μL of isooctane then dried under nitrogen stream. Five hundred ul of 1.62 M HCl-MeOH (5%, v/v) was added into each sample without or with saponification for a two-hour incubation at 50°C to generate fatty acid methyl eaters (FAMEs). After extraction twice with 500 μL of hexane, the FAMEs were dried under nitrogen stream and then dissolved in hexane. GC-MS was performed on the Thermo Scientific™ TRACE™1300 Gas Chromatography Mass Spectrometry system equipped with a TraceGOLD TG-5MS column (30 m × 0.25 mm I.D., 0.25 μm film thickness) and a ISQ LT Single Quadrupole Mass Spectrometer (Thermo Fisher Scientific). Selective ion monitoring (SIM) of a fragment with m/z of 91.1 was used for quantifying the unsaturated fatty acids by comparing the relative amount to C16:0. Selective time monitoring (STM) combined with SIM were used for quantifying ω-3 PUFAs in samples from fish oil-treated animals and the results were normalized to C19:0.

Transmission electron microscopy (TEM)

Epididymal adipose tissue was cut into one mm^3 cubes and fixed with 2.5% glutaraldehyde in 0.1 M sodium cacodylate-HCl buffer (pH 7.4) at 4°C. The fixed tissues were transferred to the cacodylate buffer containing 1% osmium tetroxide (OsO4) and incubated for one hour at room temperature. Tissue blocks were infiltrated with epoxy resin/propylene oxide (1:1 v/v) for 1.5 h and then epoxy resin for one hour at 37°C, followed by dehydration with ethanol and propylene oxide. Ultra-thin sections (100 nm) were prepared for staining with 2% aqueous uranyl acetate and Reynold's lead citrate. For immunogold staining, 100 nm ultra-thin sections were mounted on nickel grids and etched in 10% aqueous H_2O_2 for 10 minutes at room temperature. After blocking, sections were incubated with the primary antibodies overnight at 4°C, washed and transferred to a solution containing secondary antibody conjugated with 10 nm gold particles. The images were captured using a Philips CM100 transmission electron microscope (Philips, Eindhoven, the Netherlands). The average area of mitochondria was analyzed and quantified by ImageJ (Ver 1.53, NIH, USA) (Lam et al., 2021).

Western blotting

Equal amounts of proteins were separated by SDS-PAGE and transferred to polyvinylidene difluoride membranes. After overnight blocking, various primary antibodies were added for 16 h incubation at 4°C followed by detection with HRP-conjugated secondary antibodies. Immunoreactive antibody-antigen complexes were visualized with the enhanced chemiluminescence reagents from GE Healthcare (IL, USA). The relative abundance of protein bands was quantified and analyses by ImageJ.

Quantitative polymerase chain reactions (QPCR)

Total RNA was isolated using the Trizol Reagent (Thermo Fisher Scientific). The purity and concentration were evaluated by measuring the absorbance at 260 nm and 280 nm with NanoDrop 2000 (Thermo Fisher Scientific). The 260/280 ratios for all samples were between 1.8 and 2.0. The cDNA was synthesized using a PrimeScript RT reagent Kit (Takara Bio Inc., Shiga, Japan). QPCR were performed using the SYBR Green PCR Master Mix (Qiagen, Venlo, the Netherlands) on StepOnePlus™ Real-Time PCR System (Applied Biosystems, Foster City, CA, USA). Primers are listed in Table S4. Quantitation of target genes was achieved using ΔCt values after normalization with 18S ribosomal RNAs as a reference control. The fold changes were calculated for comparison between different groups.

QUANTIFICATION AND STATISTICAL ANALYSIS

Data are presented as means ± SEM. For multiple comparisons, the differences were analyzed by one-way ANOVA followed by LSD test or two-way ANOVA followed by the Bonferroni post hoc test (GraphPad Prism 8.0.2 Software, Inc., San Diego, CA, USA). Differences in other comparisons were determined by unpaired two-tailed Student's *t*-test. In all cases, statistically significant differences were accepted when *p* values were less than 0.05. All results were derived from at least three independent experiments unless otherwise specified.